AuPS/ASB Meeting - Newcastle 2007

Lunch and Posters

Tuesday 4 December 2007 – Concert Hall

Solvent dependence of the photochemistry of the voltage-sensitive fluorescent membrane probe RH421

T.H.N. Pham and R.J. Clarke, School of Chemistry, University of Sydney, Sydney NSW 2006, Australia.

Voltage-sensitive fluorescent styryl dyes, such as RH421 and di-8-ANEPPS, have attracted great interest as a means of optical imaging of electrical field strength within living cells, visualizing electrical transients in neurons and for the investigation of the reaction mechanisms of ion pumps, for example, the Na^+,K^+-ATPase. In spite of the significant advances that they have no doubt allowed, they do have some drawbacks. The most notable ones are their phototoxicity and their photochemical instability. In order to overcome these drawbacks and synthesize improved dyes, fundamental studies of their photochemical behaviour are required. This is the purpose of our study.

On illumination of solutions of RH421 with 577 nm light from a mercury lamp we have found that the dye undergoes two separate photochemical reactions, one producing a fluorescence increase and the other producing a fluorescence decrease. The amplitude of the fluorescence decrease is very dependent on the polarity of the environment, becoming increasingly less pronounced as the solvent polarity decreases and almost disappearing when the dye is bound to a lipid membrane. The fluorescence increase, on the other hand, is virtually independent of solvent polarity. This reaction has been attributed to a single-photon excited state photoisomeriastion of the dye (Amoroso *et al.*, 2006). The origin of the fluorescence decrease is unclear at this stage, but the fact that it is more prominent in polar solvents such as water and that its amplitude increases with time following addition to water suggest that it may be related to dye aggregation.

Amoroso S, Agon VV, Starke-Peterkovic T, McLeod MD, Apell H-J, Sebban P & Clarke RJ. (2006) *Photochemistry Photobiology*, **82:** 495-502.

Fitting light saturation curves measured using PAM fluorometry

R.J. Ritchie, School of Biological Sciences, The University of Sydney, NSW 2006, Australia.

Blue diode PAM (P ulse A mplitude M odulation) fluorometry was used to measure photosynthesis in *Synechococcus* (classical Cyanobacteria), *Prochlorothrix* (Prochlorophyta), *Chlorella* (Chlorophyta), *Rhodomonas* (Cryptophyte), *Phaeodactylum* (Bacillariophyta) and *Acaryochloris* (Chl d/a cyanobacteria). Effective quantum yield (F_v) *vs.* irradiance (E) curves could be described by a simple exponential decay function ($F_v = F_{vmax}e^{-kE}$) although Log/Log transformation was sometimes found to be necessary to obtain the best fits. Photosynthesis (P) was measured as Electron Transport Rate (ETR) standardised on a chlorophyll basis. P *vs.* E curves were fitted to the waiting-in-line function (an equation of the form $P = P_{max}\bullet k\bullet I\bullet e^{-kE}$) allowing 1/2 saturating and optimal irradiances to be estimated. At twice optimal light intensities there is 26.4% photoinhibition of P_{max} and is the irradiance at which all PSII would be "closed". The waiting-in-line model was found to be a very good descriptor of photosynthetic light saturation curves and superior to hyperbolic functions with an asymptotic saturation point (Michaelis-Menten, exponential saturation and hyperbolic tangent). The exponential constants (k) of the Y_v *vs* E and P *vs.* E curves should be equal because ETR is directly proportional to $Y_v \times E$. Non-Photochemical Quenching (NPQ) in *Synechococcus* was not significantly different to zero but NPQ *vs* E curves for the other algae could be fitted to an exponential saturation model.

Seasonality of chlorophyll b presence in core complexes of photosystem II from higher plants. A role of photoprotection?

P.J. Smith, N. Cox, R. Steffen, J.L. Hughes, E. Krausz and R.J. Pace, School of Chemistry, College of Science, Australian National University, Science Rd, Acton, ACT 2601, Australia.

Using two distinct and separate detergent solubilisation procedures, and Fast Phase Liquid Chromatography, a protocol for the isolation of the fully functional Core Complex of Photosystem II from higher plant spinach has been defined (Smith *et al.*, 2002). More recently, examination of Core Complexes prepared using alternative higher plant species, capsicum and silverbeet, and from spinach grown at different seasons (January – mid summer – and July – mid winter) has been undertaken. The seasonal variations for spinach were marked, with differences in capability of separating the Core Complex from Inner Light Harvesting peptides discovered. Core complexes from winter grown spinach were found to contain very low levels of chlorophyll b, indicative of rapid and efficient solubilisation of CP26 and CP29 from the Core complex using dodecyl-b-D maltoside. Cores isolated from summer grown spinach retained significant levels of chlorophyll b, indicative of a stronger interaction between CP26 and CP29 and the Core complex. Other higher plant species, typically harvested from summer grown plant material, were found to retain significant levels of chlorophyll b. This initial report characterises biochemical and biophysical parameters associated with Photosystem II core complexes and forwards an hypothesis for retention of CP26 and CP29 in summer grown higher plants, these chlorophyll containing peptides being retained for a photoprotective role.

Smith PJ, Peterson S, Masters VM, Wydrzynski T, Styring S, Krausz E & Pace RJ. (2002) *Biochemistry*, **41:** 1981-9.

Towards the structure of the β4 subunit ectodomain of the human BK K^+ channel

O.B. Clarke and J.M. Gulbis, The Walter and Eliza Hall Institute, 1G Royal Pde, Parkville 3050 VIC, Australia.

Potassium channel proteins form tetrameric pores in the membrane that facilitate the rapid, selective efflux of potassium ions across the cell membrane. Regulated potassium efflux is of fundamental importance in electrical signalling, but it also plays a role in a diverse range of other signalling pathways. The large-conductance Ca^{2+} activated potassium channel, or BK channel, is intimately involved in the regulation of calcium signalling pathways, most notably in providing a negative-feedback mechanism to regulate the activity of L-type-voltage-dependent calcium channels (VDCCs), preventing runaway Ca^{2+} influx. The physiological consequences of this simple regulatory loop are diverse; from vasodilation, to neurosecretion, to neuronal excitability, the BK channel has a variety of physiological roles, each of which requires the channel to have different electrophysiological properties. The phenotypic diversity of the BK channel is mediated, in large part, by association with a class of tissue-specific transmembrane regulatory proteins, the BK β-subunits. These proteins have diverse effects on the molecular properties of the channel. To understand how β-subunits interact with BK channels would be greatly aided by knowing their structure. The β-subunits share a two-transmembrane domain topology with short intracellular termini and a disulfide-bridged extracellular domain that is conjectured to form a novel extracellular gating ring for the BK channel (Zeng *et al.*, 2003).

To resolve the ambiguities surrounding the structure and function of the β-subunits, we aimed to determine the structure of the ectodomain of one of these proteins, the β4-subunit of the human BK channel. Here, we report the expression, refolding and crystallisation of the β4-subunit ectodomain and discuss progress towards structure determination.

We are producing the β4-subunit ectodomain by heterologous expression in *E. coli* followed by purification and refolding of the recombinant protein. Crystals were obtained and a complete native dataset collected. We were able to generate crystals derivatised with Ta_6Br_{14} by soaking this compound into the crystals. Derivatisation resulted in an unusual shift in the symmetry of the crystals – the native crystals were orthorhombic, while the Ta_6Br_{14} derivatives appeared tetragonal. Attempts to utilise the anomalous signals of tantalum and bromine for phasing by single-wavelength anomalous difference (SAD) techniques are currently underway.

We hope that the structure of the β-subunit ectodomain will shed some light on the molecular mechanisms by which transmembrane β-subunits influence BK channel gating.

Zeng XH, Xia X & Lingle CJ. (2003) *Nature Structural Biology*, **10:** 448-454.

Monitoring reaction kinetics of starch by NMR spectroscopy

A.C. Dona, School of Molecular and Microbial Biosciences, University of Sydney, NSW 2006, Australia.

The glycemic index (GI) is a measure of the rate at which glucose sugar is absorbed into the circulatory system after a meal, thus providing body fuel (Brand-Mille *et al.*, 2002). The GI of a food is related to a person's physical disposition and satiety after a meal and is used as a measure of health-status including obesity and diabetes (Jenkins *et al.*, 2002). Hypothetically, starch's structure in foods, determines its rate of digestion. However, correlating the glucose digestion process with the characteristics of the starch in food remains to be studied. Characterisation of starch samples by techniques including nuclear magnetic resonance (NMR) (Le Botlan & Desbois, 1995) and size exclusion chromatography (SEC) require a stable starch solution.

NMR is one technique that can be used to study the dissolution kinetics of complex mixtures, including starch in various solvents (DMSO:H_2O) at different temperatures. The kinetics of dissolution were studied using the intensity of peaks in NMR spectra that increased as starch dissolved. Rate constants for dissolution were determined in the temperature range 30°C-80°C. Arrhenius analysis was used to estimate the activation energy of dissolution. Complete dissolution was confirmed by using dynamic light scattering (DLS).

The kinetics of the reactions involved in digestion of starch

$$\text{Starch} + \text{Glucoamylase} \rightarrow \beta\text{-glucose} \leftrightarrow \alpha\text{-glucose}$$

in aqueous solutions were monitored. ^{1}H NMR generated progress curves in a more direct way than conventional glucose assay methods (Wang *et al.*, 2006). In addition the amount of α and β glucose released and that then underwent mutarotation (Figure) were quantified. Estimates of rate constants that describe the kinetics of the dissolution process and the mutarotation of the anomers were obtained by nonlinear regression in *Mathematica*. The kinetic model will be used to correlate starch-digestion rates measured *in vitro* with the GI measured *in vivo*

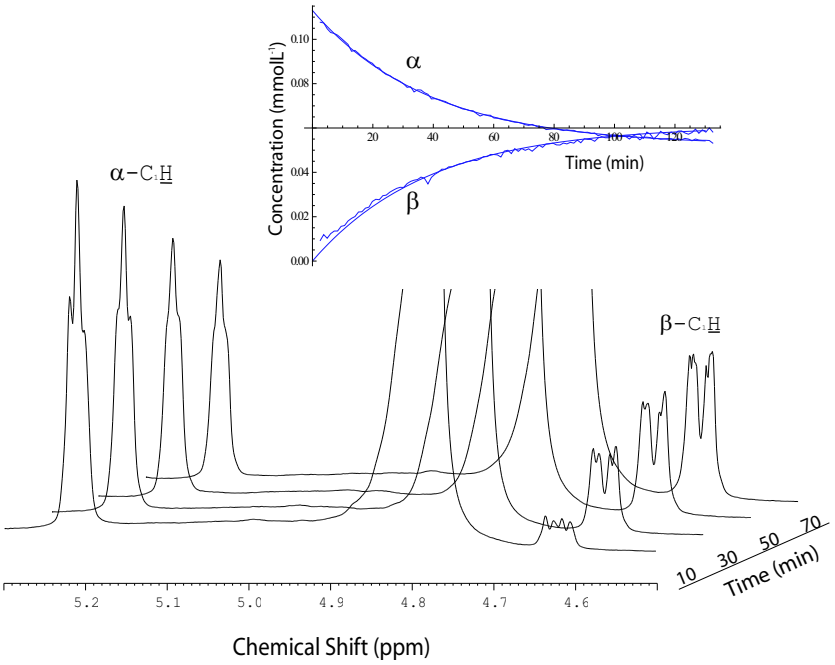

The figure shows ^{1}H NMR (400.13MHz) time course of spectra showing the mutarotation of α-D glucose to β-D glucose. Temperature was 25°C, Acetate buffer pH 5.2. NMR parameters: π/2 pulse duration 8 μs, number of transients per spectra 8, a line broadening of 0.3Hz was applied to each fid before Fourier transformation. *Inset:* Progress curves showing the conversion of the α-anomer to the β-anomer.

Brand-Miller JC, Holt SHA, Pawlak DB & McMillan J. (2002) *American Journal of Clinical Nutrition*, **76:** 281S-5S.

Jenkins DJA, Kendall CWC, Augustin LSA, Franceschi S, Hamidi M, Marchie A, Jenkins AKL & Axelsen M. (2002) *American Journal of Clinical Nutrition*, **76:** 266S-73S.

Le Botlan D & Desbois P. (1995) *Cereal Chemistry*, **72:** 191-3.

Wang JP, Zeng AW, Liu Z & Yuan XG. (2006) *Journal of Chemical Technology and Biotechnology*, **81:** 727-9.

Muscling in on Paramagnetic NMR

N.M. Cordina,[1] J.A. Cooke,[1] M.W. Howell,[1] J.M. Mackay[2] and L.J. Brown,[1] [1]Department of Chemical and Biomolecular Sciences, Macquarie University, North Ryde NSW 2109, Australia and [2]School of Molecular and Microbial Biosciences, University of Sydney, NSW 2006, Australia.

The calcium-mediated regulation of striated muscle contraction is of critical importance in vertebrates, and at the core of this complex regulatory system is Troponin (Tn). In the absence of calcium, this large, flexible protein inhibits actin-myosin interaction. However, upon calcium binding, Tn undergoes a large conformational change, enabling actin-myosin interaction and thus muscle contraction to occur.

The mobility of Tn complicates structural and mechanistic studies of the protein. Therefore, the emerging method of structure analysis, Paramagnetic Relaxation Enhancement NMR (PRE), has been investigated for its application to Tn. The PRE technique requires a paramagnetic compound, which contains an unpaired electron, to be incorporated into the protein for NMR studies. Site directed spin labelling (SDSL) is used to attach a spin label, such as a nitroxide group, to the cysteine residue of the protein via a disulfide bond.

In the 15N-HSQC NMR experiments, the unpaired electron of the paramagnetic nitroxide spin label interacts with nearby spin nuclei, causing a distance dependent increase in relaxation rate of nuclei within a ~25 Å radius. This PRE effect is observed in the HSQC spectra as peak broadening. The distance between the affected nucleus and the spin label can be determined from the magnitude of this broadening, as described by the Solomon–Bloembergen equation (Solomon, 1955). PRE can thus be used to obtain long-range distance constraints, which enables inter-domain movements to be detected. This method is therefore useful in examining the large conformational change that occurs in Tn upon calcium binding.

To examine the suitability of SDSL-PRE for troponin studies, we have produced four single cysteine (Cys) mutants of the small calcium-binding subunit of cardiac Tn, Troponin C (TnC – Cys35, Cys84, Cys94 and Cys136) by site directed mutagenesis. The TnC N15 mutants are labelled with the nitroxide spin label (MTSSL) and HSQC spectra acquired in the paramagnetic and reduced states of the spin label. Potential NMR experiments are to collect PRE data for each mutant in the presence and absence of calcium to compare conformational changes in TnC between the two states. The four TnC mutant cysteine locations provide an overview of the conformational changes that occur in TnC upon calcium binding.

Solomon I. (1955) *Physical Review*, **99:** 559–65.

Rotation of some mutants of thermophilic F_1-ATPase

M.D. Hossain,[1,2] S. Furuike,[1] Y. Maki,[3] K. Adachi[1] and K. Kinosita Jr.,[1] [1]Department of Physics, Faculty of Science and Engineering, Waseda University, Okubo 3-4-1, Shinjuku-ku, Tokyo 169-8555, Japan, [2]Department of Physics, School of Physical Sciences, Shahjalal University of Science and Technology, Sylhet-3114, Bangladesh and [3]Department of Physics, Osaka Medical College, Osaka 569-8686, Japan. (Introduced by S. Bröer)

A single molecule of F_1-ATPase works as a rotary protein motor. It is a water soluble portion of the ATP synthase that catalyzes the synthesis of adenosine tri-phosphate (ATP) in animals, plants and bacteria. The minimal stable sub-complex of F_1-ATPase for catalysis consists of $\alpha_3\beta_3\gamma$ subunits. A high resolution structure of bovine mitochondrial F_1-ATPase (MF_1) determined by Abrahams *et al.* (1994), has revealed that three α- and three β-subunits are alternately arranged to form a stator cylinder. Three β subunits bind and hydrolyze ATP whereas three α subunits bind ATP without hydrolysis. An α-helical coiled coil made of the amino- and carboxy-termini of the γ-subunit deeply penetrates the central cavity of the stator cylinder and is held by the cylinder wall at two positions, at the orifice and the bottom. The tip of the carboxy-terminus of the γ-subunit held by the bottom of the stator cylinder was suggested to play important roles in rotation of γ-subunit. Whether the tip of γ subunit plays any role in rotation, however, remains an intriguing question. In this study, an $\alpha_3\beta_3\gamma$ sub-complex of F_1-ATPase derived from thermophilic Bacillus PS3 (TF_1) having a structure similar to MF_1 was expressed in *Escherichia coli*. The γ-subunit was genetically truncated both at its amino- and carboxy- termini step by step until the remaining rotor portion would be outside the stator cavity and simply sit on the concave entrance of the stator orifice. Rotation of the wild type and mutants were observed adopting single molecule techniques. It was found that all truncation mutants rotated in the correct direction, though some mutants exhibited moments of irregular motion. The time-averaged rate of rotation as well as the rate of ATP hydrolysis was low in the mutants compared to the wild type, indicating that most of the interactions between the rotor and the stator cylinder are important for the rapid progress of catalysis. These interactions, however, are not essential for rotation.

Abrahams JP, Leslie AGW, Lutter R & Walker JE. (1994) *Nature*, **370:** 621-8.

Ratchets: Rectifying Brownian motion for transport

S.J. Lade and Y.S. Kivshar, Nonlinear Physics Centre, Research School of Physical Sciences and Engineering, The Australian National University, ACT 0200, Australia.

A major reason for the great resurgence of interest in ratchets – broadly, systems capable of rectifying unbiased fluctuations into directed transport – about 10 years ago was for their possible role in explaining the operation of molecular motors such as kinesin. Kinesin contrives to 'walk' along the cytoskeleton, without any external force to bias its motion. A number of 'Brownian motor' ratchet models were proposed to explain how kinesin and other molecular motors such as myosin and the rotary F1-ATPsynthase achieve this transport. Some of these models were of an appealing but speculative nature (Menche & Schimansky-Geier, 2006), others general in scope (Reimann, 2002; Ait-Haddou & Herzog, 2003), while some claimed to reproduce specific experimental results (Derényi & Vicsek, 1998). The lack of detailed information about the motors' conformations and dynamics, however, mean that current efforts to explain their motion are returning to conventional discrete chemical models (Kolomeisky & Fisher, 2007).

The generality of the ratchet concept, however, suggests potential applications in biophysics beyond just molecular motors. A primary task of this poster is to provide a review of general ratchet types and properties. From a theoretical viewpoint, there are two basic classes of ratchets: rocking and flashing. In the rocking ratchet, a periodic zero-mean force is applied to the particle (or variable being modeled as a particle), which in turn is moving in a periodic potential 'landscape'. A flashing, or pulsating, ratchet has no external force but has the potential landscape depending on time. This time dependence could be deterministic or stochastic. Rocking ratchets are the most straightforward to implement in nanotechnology, while pulsating ratchet models are often more suitable for biophysics, being able, for example, to model stochastic switching between chemical states (Reimann, 2002), and are the form most commonly employed in modeling molecular motors. If the particle is moving in a two-dimensional asymmetric potential, like the 'Christmas tree' potential, it is known as a geometric ratchet. Such models beckon comparison with transport in ion channels; this is reinforced by geometric ratchet-like models showing negative resistance in response to an applied force (Cecchi & Magnasco, 1996), an important feature of some ion channels.

All ratchets share the capability of rectifying unbiased fluctuations into directed transport through a breaking of symmetry. This is most commonly the spatial symmetry of the potential, but transport is also achievable by breaking of temporal symmetry. Despite that at a coarse-grained level, the potential is completely flat, particle transport will occur. The direction of transport, however, is often not obvious; indeed, in many ratchets the current direction may completely reverse on the variation of some system parameter. Ratchet models, particularly pulsating models, may also have the particle undergoing Brownian motion; the ratchet may then be called a 'Brownian ratchet' or 'Brownian motor'.

This ratchet phenomenon is sufficiently general and appealing – this directed transport where one might expect none – that it has found, and one might reasonably expect it to find, application in varied areas of biophysics and physics and general. It is hoped that the concepts presented in this review will allow the biophysicist to see phenomena from their own study in this new framework and possibly apply results and ideas from this emerging field.

Menche J & Schimansky-Geier L. (2006) *Physics Letters A,* **359:** 90-98.
Reimann P. (2002) *Physics Reports,* **361:** 57-265.
Ait-Haddou R & Herzog W. (2003) *Cell Biochemistry and Biophysics,* **38:** 191-213.
Derényi I & Vicsek T. (1998) *Physica A,* **249:** 397-406.
Kolomeisky AB & Fisher ME. (2007) *Annual Review of Physical Chemistry,* **58:** 675-695.
Cecchi GA & Magnasco MO. (1996) *Physical Review Letters,* **76:** 1968-1971.

Modelling *Staphylococcus aureus*-induced septicemia using NMR

R. Plummer,[1] J. Bodkin,[2] T.W. Yau ,[1,4] D. Power,[3] N. Pantarat,[3] T.J. Larkin,[1] D. Szekely,[1] W.A. Bubb,[1] T.C. Sorrell,[3] C.J. Garvey[4] and P.W. Kuchel,[1] [1]School of Molecular and Microbial Biosciences, University of Sydney, NSW 2006, Australia, [2]School of Chemistry, University of New South Wales, NSW 2052, Australia, [3]Centre for Infectious Diseases and Microbiology, University of sydney and Westmead Millennium Institute, Westmead, NSW 2145, Australia and [4]Australian Nuclear Science and Technology Organisation, Menai, NSW 2234, Australia.

We present a novel NMR-based study of the molecular aspects of the "attack" on human red blood cells (RBCs) by growing bacteria. *Staphylococcus aureus* expresses virulence factors, including α-haemolysin, which contribute to the clinical condition known as septic shock (Bhakdi & Tranum-Jensen, 1991). α-Haemolysin is a pore-forming toxin and its secretion increases the permeability of a range of mammalian cell types infected with *S. aureus* (McEwen & Arion, 1985). ^{31}P NMR spectra of the probe molecules dimethyl methylphosphonate (DMMP) and hypophosphite (HPA) in RBC suspensions show separate intra- and extracellular resonances (Kirk & Kuchel, 1986). These resonances coalesced over time in RBC suspensions inoculated with *S. aureus* or pure α-haemolysin, due to increasing permeability of the RBC membrane. Increased RBC permeability resulted in leakage of intracellular proteins, plus an increase in the exchange rates of the solutes between the intra- and extracellular compartments, both effects contributing to the coalescence of the split peaks (Plummer *et al.*, 2007). The addition of antibiotics prevented peak coalescence and enabled the minimal inhibitory concentration (MIC) for eight strains of *S. aureus* to be determined for oxacillin and erythromycin. The MIC values obtained by using ^{31}P NMR spectroscopy were within one dilution of the MICs obtained using the standard National Committee for Clinical Laboratory Standards (NCCLS) method (Jones, 1986). The results are encouraging for the use of NMR spectroscopy in clinical microbiology.

Bhakdi S & Tranum-Jensen J. (1991) *Microbiological Reveiews*, **55:** 733-51.
McEwen BF & Arion WJ. (1985) *Journal of cell Biology*, **100:** 1922-9.
Kirk K & Kuchel PW. (1986)*Journal of Magnetic Resonance*, **68:** 311-8.
Plummer R, Bodkin J, Yau TW, Power D, Pantarat N, Larkin TJ, Szekely D, Bubb WA, Sorrell TC & Kuchel PW. (2007) *Magnetic Resonance in Medicine*, **58:** 656-65.
Jones RN. (1986) *Antimicrobic Newsletter*, **3:** 1-7.

pH behaviour of the water chemical shift in ^{1}H NMR of red cells with low transmembrane magnetic susceptibility difference

T.J. Larkin, W.A. Bubb and P.W. Kuchel, School of Molecular and Microbial Biosciences, University of Sydney, NSW 2006, Australia.

The ^{1}H magic angle spinning (MAS) NMR spectrum of water in erythrocyte suspensions shows peaks from each of the intracellular and extracellular water pools. The splitting is a true chemical shift and is brought about by the elimination of water exchange under MAS conditions due to physical separation of the two water populations. The size of the chemical shift difference is determined by the concentration of intracellular protein affecting the average extent of hydrogen bonding of water (Larkin *et al.*, 2007). We present here a model of the chemical shift behaviour for water in erythrocytes under normal high resolution NMR conditions based on results from MAS experiments on these cells exposed to different pH and osmotic conditions. The model accurately predicts the chemical shift of water for a static sample, and the results demonstrate that in high resolution NMR experiments the chemical shift of water will appear to be invariant if differences in magnetic susceptibility across the cell membrane are minimal (< 10% of the magnetic susceptibility of water). Thus changes in the shape and chemical shift of the water resonance are not due to pH changes in the physiological range (6-8). The findings are fundamental to an interpretation of the mechanism of chemical shift effects on the water resonance that may occur in functional magnetic resonance imaging.

Larkin TJ, Bubb WA & Kuchel PW. (2007) *Biophysical Journal*, **92:** 1770-6.

The ability of the red blood cell to synthesise glutathione in type 2 diabetes mellitus, and the implications for disease management

S. Whillier,[1] J.E. Raftos[1] and P.W. Kuchel,[2] [1]Department of Biological Sciences, Macquarie University, NSW 2109, Australia and [2]School of Molecular and Microbial Biosciences, The University of Sydney, NSW 2006, Australia.

Both the pathogenesis and complications of type 2 diabetes mellitus (NIDDM) have been associated with oxidative stress. Abdominal obesity and associated inflammation prior to the development of NIDDM is an oxidative stress that causes insulin resistance and deterioration of the β-cells of the pancreas. Hyperglycemia produces oxidative stress by promoting non-enzymatic glycation, glucose autoxidation (glycoxidation), and the formation of advanced glycation end products (AGE) and reactive oxygen species (ROS). Cells have antioxidant systems to deal with ROS, but high oxidative stress implies an inability of these systems to cope with the oxidative load.

The tripeptide glutathione (GSH) (γ-glutamyl cysteinyl glycine) is a ubiquitous intracellular antioxidant and is considered to be the largest mobile antioxidant pool and detoxifier. A decrease in GSH concentration in the red blood cells (RBCs) of diabetes subjects is widely reported. However, several authors report unchanged or elevated GSH concentrations in diabetes.

In this study, RBCs taken from 20 NIDDM subjects (58.3 ± 2.5 yr) with a mean HbA_{1c} of 8.34 ± 0.2%, and 20 healthy controls (46.6 ± 3.3 yr) with a mean HbA_{1c} of 5.7 ± 0.1% were GSH-depleted using 1-chloro-2,4-dinitrobenzene, and then incubated in a solution containing substrates for GSH synthesis (alanine, α-ketoglutarate, glycine and N-acetyl cysteine), and sampled for total free GSH using a DTNB/enzymatic recycling procedure . The NIDDM subjects had the same total free GSH concentration (1.89 ± 0.1 *vs.* 1.91 ± 0.1 mmol(L RBC)$^{-1}$), and the same rate of GSH synthesis (1.14 ± 0.1 *vs.* 1.06 ± 0.1 μmol(L RBC)$^{-1}$(min)$^{-1}$) as controls ($p > 0.05$), indicating that the GSH synthesizing enzymes were normal. NIDDM, but not controls, showed an increase in total GSH concentration ($p = 0.0001$ for slope, ANCOVA for TFG, $F_{(1,38)} = 7.5624$, $p = 0.0093$) and a trend toward increasing rates of GSH synthesis ($p = 0.09$) with increasing age, not related to the amount of glycation, as the HbA_{1c} was not well-correlated with age. Healthy controls had a positive correlation between the rate of GSH synthesis and total GSH concentration ($p = 0.0005$, $r = 0.71$). NIDDM subjects did not ($p = 0.731$, $r = 0.05$), indicating larger oxidative loads.

To our knowledge, our results provide the first evidence that intact RBCs from NIDDM subjects, given adequate substrate, are able to synthesise GSH at normal rates compared to healthy, age-matched controls.

What are the roles of amino acid transporters B^0AT1 and ASCT2 in kidney and intestine?

N. Tietze and S. Bröer, School of Biochemistry and Molecular Biology, Australian National University, ACT 0200, Australia.

In both kidney and intestine neutral amino acids are absorbed by a major transport activity specific for this class of amino acids, referred to as system B^0. Two different amino acid transporters have been suggested to mediate this activity, namely B^0AT1 (SLC6A19) and ASCT2 (SLC1A5). B^0AT1 (SLC6A19) is an apical neutral amino acid transporter in mammalian kidney and intestine. Amino acid transport mediated by B^0AT1 is sodium dependent, chloride independent and pH sensitive (Bröer *et al.*, 2004). Further studies revealed the transport mechanism as a cotransport of Na^+ and substrate with a stochiometry of 1:1 (Bohmer *et al.*, 2005). It has been shown that dysfunction of B^0AT1 is responsible for Hartnup disorder, an autosomal recessiv disorder of neutral amino acid absorption (Kleta *et al.*, 2004; Seow *et al.*, 2004).

ASCT2 (SLC1A5) (Avissar *et al.*, 2001; Kekuda *et al.*, 1996) also mediates transport of neutral amino acids except those with aromatic side chains. ASCT2 is a Na^+ dependent, electroneutral antiporter. At low pH, ASCT2 also accepts glutamate and aspartate. Expression of ASCT2 has been reported in the apical membrane of kidney proximal tubules and the intestine. These localization results indicate that both ASCT2 and B^0AT1 could contribute to neutral amino acid absorption in kidney and intestine. In the acidic microclimate of the intestine ASCT2 could also contribute to glutamate uptake, which would be absorbed in exchange for neutral amino acids. B^0AT1 could then recapture the neutral amino acids constituting a tertiary active transport system. The aim of this study is to determine the role of the two amino acid transport B^0AT1 and ASCT2 in kidney and in intestine.

To investigate the contribution of the two transporters, renal and intestinal brush border vesicles from mice were generated. Alkaline phosphatase enrichment suggested an 8-9-fold enrichment of the apical membrane. This was supported by Western Blots showing enrichment of the apical transporter B^0AT1. However, significant amounts of the basolateral marker 4F2hc were observed as well. Uptake of leucine was studied in the presence of phenylalanine, glutamine and alanine to discriminate between the two transporters. Competition of leucine transport was observed with all three amino acids. The data obtained from vesicle studies were compared with the properties of B^0AT1 and ASCT2 when expressed in *Xenopus laevis* oocytes.This comparison showed that leucine uptake was nearly completely inhibited by the B^0AT1 substrate phenylalanine in kidney.

Avissar NE, Ryan CK, Ganapathy V & Sax HC. (2001). *American Journal of Physiology: Cell Physiology*, **281:** C963-71.

Bohmer C, Bröer A, Munzinger M, Kowalczuk S, Rasko, JE, Lang F & Bröer S. (2005) *Biochemical Journal* **389:** 745-51.

Bröer A, Klingel K, Kowalczuk S, Rasko JE, Cavanaugh J & Bröer S. (2004). *Journal of Biological Chemistry*, **279:** 24467-76.

Kekuda R, Prasad PD, Fei YJ, Torres-Zamorano V, Sinha S, Yang-Feng TL, Leibach FH & Ganapathy V. (1996) *Journal of Biological Chemistry*, **271:** 18657-61.

Kleta R, Romeo E, Ristic Z. *et al.* (2004). *Nature Genetics*, **36:** 999-1002.

Seow HF, Bröer S, Bröer A, Bailey CG, Potter SJ, Cavanaugh JA & Rasko JE. (2004) *Nature Genetics*, **36:** 1003-7.

What is the physiological role of the neurotransmitter transporter 4 (NTT4) in the central nervous system?

S. Balkrishna and S. Bröer, School of Biochemistry & Molecular Biology, Australian National University, ACT 0200, Australia.

The neurotransmitter transporter 4 (NTT4) is a member of the solute carrier family 6 (SLC6) or the neurotransmitter transporter family of membrane transporters. Members of this family have a significant physiological relevance and have been implicated in several disorders and conditions such as anxiety, epilepsy, attention deficit hyperactivity disorder (ADHD), cocaine addiction, obesity, and Hartnup disorder (Brõer, 2006).

NTT4 (SLC6A17) is distributed widely across the central nervous system in the pre-synaptic axon terminals of most glutamatergic and a small sub-section of GABAergic neurons (el Mestikawy *et al.*, 1997). It belongs to the branch of "orphan" transporters, which was initially called so because the function of the members of this branch could not be identified. However, since the identification of SLC6A15, SLC6A19 and SLC6A20 as amino acid transporters, it is alleged that the orphan transporters might in fact all be transporters of amino acids (Brõer, 2006). Although NTT4 is a member of this amino acid transporter branch, its function is still unknown. The aim of this study was to identify substrate(s) transported by NTT4, and thus hypothesize its function in the central nervous system.

*Xenopus laevis** oocytes were chosen as an appropriate expression system to study the function of the transporter. Confocal microscopy on oocytes expressing eGFP- NTT4 suggested that the transporter was expressed on the oocyte surface membrane. This was further confirmed by the surface biotinylation of oocytes expressing NTT4.

Radioactive uptake experiments initially suggested that the uptake of radiolabeled leucine, proline, glycine and glutamine was significantly higher in oocytes expressing NTT4 as compared to non-injected oocytes. To confirm that this uptake was due to NTT4, a conserved arginine residue (R85) was mutated to serine in an attempt to make the transporter non-functional. However, uptake of labelled leucine, proline, glycine and glutamine was still observed in oocytes expressing NTT4-R85S.

To confirm that the R85S mutation made the transporter non-functional, the same mutation was created in SLC6A15 (B0AT2), the closest homolog of NTT4. Radioactive uptake of proline showed that the R85S mutation reduced transport activity to background levels. To further analyse if NTT4 needed to be modified to be functional, two putative phosphorylation sites were identified. These two residues were mutated and the uptake of leucine, proline, glycine and glutamine was measured. However, there was no significant difference in the uptake of these amino acids in oocytes expressing the wild type and phosphorylation mutants of NTT4.

Although the function of NTT4 is still unknown, further studies using electrophysiology and potential protein interactions of the transporter could elucidate its role in the central nervous system.

Brõer S. (2006) *Neurochemistry International*, **48:** 559-67.
el Mestikawy S, Wehrle R, Masson J, Lombard MC, Hamon M & Sotelo C. (1997) *Neuroscience*, **77:** 319-33

---

* Procedures to remove oocytes were approved by the animal ethics committee of the ANU.

The role of the EGF receptor in albumin-induced renal fibrosis

Y. Jang, C. Slattery and P. Poronnik, School of Biomedical Sciences, The University of Queensland, Qld 4072, Australia.

During kidney disease urinary albumin levels increase dramatically. Albuminuria is recognised as an indicator of renal dysfunction is also a major mediator of renal damage and fibrosis. The mechanisms behind albumin induced-renal fibrosis are still unclear, but a number of lines of evidence suggest involvement of the epidermal growth factor (EGF) receptor. Under normal conditions, the EGF receptor plays a key role in the maintenance of normal epithelial cell function, however, inappropriate activation has been shown to have detrimental effects in a number of physiological settings. The primary aim of this study was to examine the role of the EGF receptor in albumin-induced fibrotic effects in proximal tubular cells.

Experiments were performed using the human renal proximal tubular epithelial cell line, HK-2. The effects of increasing albumin concentrations (0.1, 1 and 5mg/ml) were examined over 72 hours. Firstly, the effects of albumin on fibronectin expression were examined. Fibronectin is a major component of extracellular matrix (ECM) and is significantly increased during tubulointerstitial fibrosis. In cell lysate and cell supernatant, fibronectin protein levels were significantly increased by treatment with 1 and 5 mg/ml albumin. Fibronectin protein levels are determined by a number of factors including synthesis and proteolytic degradation by the matrix-metalloproteases (MMPs). To investigate the mechanism of fibronectin accumulation, RT-PCR analysis was performed to assess the levels of fibronectin mRNA. Albumin treatment did not significantly affect fibronectin mRNA levels suggesting that the accumulation was not a transcriptional event. MMP activity is regulated by their physiological inhibitors the tissue inhibitors of metalloproteases (TIMPs). RT-PCR analysis revealed that albumin treatment resulted in an upregulation of TIMP1 mRNA levels leading to the hypothesis that fibronectin accumulation under high albumin conditions may be due to impaired degradation due to MMP inhibition. TIMP production has previously been linked to EGF-receptor activation in the PTECs. In this current study, under high albumin conditions, phospho-EGF-receptor levels were significantly increased. Co-treatment of PTECs with high albumin and an EGF-receptor antagonist, AG1478, resulted in inhibition of albumin-induced TIMP-1 upregulation and fibronectin accumulation. Further experiments revealed that albumin-induced effects were also mediated by the ERK1/2 mitogen activated kinase pathway, downstream of the EGF-receptor.

In conclusion, the results of this study suggest that albumin-induced fibrotic effects are mediated, at least in part by activation of the EGF-receptor. These findings provide novel insights into albumin-induced renal fibrosis and further elucidation of these mechanisms may identify new potential therapeutic strategies.

Gonadotrophin hormones in flying-fox plasma during key reproductive stages

A.A. Macdonald, K.-A. Gray and G.M. O'Brien, Human Biology and Physiology, University of New England, NSW 2351, Australia.

Negative feedback from ovaries to the pituitary gland is usually achieved by oestradiol and progesterone in mammals. Counter-current exchange transfers these hormones from ovarian veins to ovaro-uterine arteries in flying-foxes (Genus *Pteropus*). As a result, information regarding the timing of ovarian activities such as ovulation cannot be achieved by measuring sex steroids in systemic plasma. The alternative approach being taken in the present study is to measure plasma concentrations of the gonadotrophins, follicle stimulating hormone (FSH) and luteinising hormone (LH), which communicate the pituitary signals to the gonads. This has not previously been attempted in any species of Megachiroptera, so reference values for both sexes of two species have been measured, to provide a basis for subsequent longitudinal investigations in individual animals during known reproductive stages.

Methods. Heterologous radioimmunoassays (RIAs) were adapted for measuring FSH and LH in plasma samples from *P. poliocephalus* and *P. scapulatus*. The assay for FSH used a polyclonal antibody (rabbit anti-ovine FSH), while the LH assay used a monoclonal antibody (mouse anti-bovine LH). Ovine hormones, oFSH and oLH, were used as standards. Plasma samples were collected by venipuncture from a cross section of captive and wild, intact and gonadectomised animals. Mean plasma concentrations of FSH and LH were compared between broad reproductive categories, by ANOVA of log transformed data.

oFSH and oLH Plasma Concentrations (ng/mL)
Mean ± SE (*n*)

FEMALES		**Folliculogenesis**		**Mating**		**Pregnancy**		***P***
P. poliocephalus	**FSH**	1.47 ± 0.61	(9)	0.53 ± 0.03	(8)	0.67 ± 0.07	(31)	0.01
	LH	2.56 ± 1.25	(7)	3.05 ± 1.72	(6)	1.77 ± 0.78	(7)	0.16
P. scapulatus	**FSH**	1.12 ± 0.31	(4)	0.87 ± 0.15	(7)	1.33 ± 0.33	(5)	0.24
	LH	1.50 ± 0.62	(5)	1.84 ± 1.05	(7)	2.09 ± 1.09	(7)	0.60
MALES		**Recrudescence**		**Mating**		**Regression**		***P***
P. poliocephalus	**FSH**	0.89 ± 0.14	(6)	0.81 ± 0.15	(13)	1.1 ± 0.22	(15)	0.73
	LH	1.48 ± 0.55	(4)	1.71 ± 0.63	(7)	1.53 ± 1.05	(9)	0.63
P. scapulatus	**FSH**	3.24 ± 1.56	(4)	1.46 ± 0.55	(9)	1.6 ± 0.86	(3)	0.54
	LH	1.80 ± 0.59	(4)	2.84 ± 1.72	(9)	2.77 ± 0.74	(3)	0.41

Results. In *P. poliocephalus* females, FSH was increased during folliculogenesis ($P < 0.01$, see Table). In *P. scapulatus* a trend toward suppression during pregnancy was weak due to small sample sizes. Plasma was available from several ovariectomised *P. poliocephalus* during the times of mating (FSH: 1.8, 2.4 ng/mL) and pregnancy (FSH: 1.03 ± 0.42, $n = 12$). In each instance these were higher than the mean in the parallel group of gonad-intact animals.

In male *P. poliocephalus* and *P. scapulatus* there were no trends in FSH or LH associated with the broad categories of testicular recrudescence, mating, and testicular regression. Removal of negative feedback by gonadectomy led to LH concentrations of 9.0 and 4.8 ng/mL in individual male *P. poliocephalus*, and 13.4 and 7.5 ng/mL in male *P. scapulatus.*

Conclusion. These preliminary data suggest that in female flying-foxes, FSH is secreted in patterns that are similar to those in other mammals. Apparent elevation of FSH during folliculogenesis suggests that FSH would be the more informative gonadotrophin to pursue in subsequent investigations into the regulation of reproduction in flying-foxes. Elevation of both gonadotrophin levels following gonadectomy confirms that pituitary hormones are under negative feedback from the gonads, as in other mammals, despite the novel vascular complex that supports the counter-current exchange of ovarian steroids.

The effect of a selective α7-nicotinic acetylcholine receptor antagonist on endothelium-dependent relaxation in rat mesenteric arteries

P.S. Chadha,[1,2] J.D. Moffatt[3] and R. Lever,[1] [1]Department of Pharmacology, The School of Pharmacy, University of London, WC1N 1AX, UK, [2]School of Medical Sciences, University of New South Wales, NSW 2052, Australia and [3]Department of Physiology, St. George's, University of London, SW17 0RE, UK.

Neuronal type nicotinic acetylcholine receptors (nAChR), in particular of the α7 subtype, are expressed on vascular endothelial cells where their function remains unclear. Endothelial cells have also been shown to possess all the components of an endogenous cholinergic system including acetylcholinesterase (AChE), choline acetyltransferase (ChAT) and the vesicular ACh transporter (VAChT) (Reviewed by Kirkpatrick *et al*., 2001). Previously, we have found that nicotine exposure has differential effects in mesenteric and pulmonary arteries where it leads to improved maximum endothelium-dependent relaxation in mesenteric vessels and an impaired response in pulmonary vessels (Chadha *et al*., 2005). In the present study, we have investigated acetylcholine-induced relaxation in rat mesenteric arteries, following exposure of vessels to the α7 nAChR-selective antagonist methyllycaconitine (MLA).

Male Wistar rats (240-260g) were killed by CO_2 asphyxiation. Third order mesenteric arteries were isolated and treated with 6-hydroxydopamine (2 mM) and capsaicin (0.1 mM) for 30 minutes, in order to remove neuronal influences. Following this, some vessels were incubated in DMEM containing MLA (10^{-7} M) both alone and in the presence of nicotine (10^{-7} M) or the VAChT inhibitor vesamicol (100 μM) and AChE (0.1 units/ml). Following 48 hours incubation, 2 mm segments of artery were mounted on a wire myograph under normalised tension in oxygenated (95% O_2/5% CO_2) Krebs' buffer maintained at 37°C. Maximum contraction to KCl (120 mM) was initially determined and ~50% maximal tone subsequently induced using phenylephrine, in the presence of nifedipine (0.3 μM), before assessment of ACh-induced relaxation. Maximal responses to ACh (E_{max}) are expressed as percent relaxation of active tone (mean ± SEM) and differences determined by ANOVA, followed by Dunnett's post test ($p < 0.05$). n = 6-7 per group.

Nicotine exposure enhanced subsequent maximal endothelial-dependent relaxation of mesenteric arteries, in response to ACh (87.2 ± 3.1% *vs.* 73.7 ± 5.4% vehicle control), an effect that was abolished by co-exposure to MLA (60.2 ± 9.3%). Interestingly, exposure of rat mesenteric arteries to the α7 nAChR-selective antagonist MLA alone augmented endothelium-dependent relaxation in response to ACh compared to vehicle control (E_{max}: 87.4 ± 2.1% *vs.* 69.5 ± 5.1%; pEC_{50}: 8.0 ± 0.1 *vs.* 7.1 ± 0.2, respectively). Moreover, the effects of MLA treatment were completely abolished following co-exposure to vesamicol and AChE (E_{max}: 65.6 ± 5.9%; pEC_{50}: 7.1 ± 0.1), whilst vesamicol/AChE treatment alone was without effect.

These data suggest that endothelial nAChRs may possess a role in control of vascular tone in rat mesenteric arteries and, furthermore, an autocrine effect of endogenous ACh may be in place, mediated in part by α7 nAChR.

Chadha PS, Moffatt JD & Lever R. (2005) *Proceedings of the British Pharmacological Society*, http://www.pa2online.org/abstracts/Vol3Issue2abst057P.pdf

Kirkpatrick CJ, Bittinger F, Unger RE, Kriegsmann J, Kilbinger H & Wessler I. (2001) *Japanese Journal of Pharmacology*, **85:** 24-28.

Synchronization of sinoatrial node cells: the effect of gap junctions

S. Polwiang and A. Coster, School of Mathematics and Statistics, The University of New South Wales, NSW 2052, Australia.

There are several mathematical models that describe the electrical activity and ion exchange in the sinoatrial (SA) node. The response of the cell to an externally applied current is to change the timing of the subsequent action potential. This change is dependent on the nature of the applied current, and also the phase, (time, relative to the unperturbed cycle), at which the perturbation is applied. Using a model SA node cell, based on a Hodgkin-Huxley formalism (Dokos *et al.*, 1996) we explored the effects of coupling cells *via* direct, gap junction connections. The simulation was implemented using Mathlab. A 4^{th} Runga-Kutta integration method used to solve the coupled differential equations. The otherwise identical cells were initialised over the entire range of initial phase differences, and connected *via* gap junctions with conductances in the range of 0-500 pS. The membrane potential of the coupled cells quickly synchronized, and preliminary results of the relationship between the time taken to synchronize *versus* both initial phase difference and gap junction conductance suggests an optimal value of gap junction conductance minimizing the synchronization time. Whilst the effect of gap junction connectivity is the major determinant in synchronization in these cells, other factors also play a role. These include electrical field effects and the effect of a shared interstitial space between the cells.

Dokos S, Celler B & Lovell N (1996) *Journal of Theoretical Biology*, **181:** 245-272. DOI 10.1006/jtbi.1996.0129

Regulatory volume decrease in isolated cardiomyocytes: differences between freshly isolated and cultured cells?

J.R. Bell, D. Lloyd and M.J. Shattock, Cardiovascular Division, King's College London, The Rayne Institute, St. Thomas' Hospital, London, SE1 7EH, U.K.

Changes in cardiomyocyte volume can have profound effects on contractile function and have been suggested to contribute to the pathophysiology of ischemia/reperfusion injury. There is extensive evidence that many different cell types regulate their volume in response to hypo-osmotic-induced cell swelling, employing a series of signaling pathways to promote extrusion of intracellular osmolytes and to facilitate the movement of water out of the cell (regulatory volume decrease, RVD). Reports of cell volume regulation in isolated cardiomyocytes have varied depending on the model used. Cultured chick cardiomyocytes consistently show RVD, in contrast to conflicting reports in freshly isolated, adult mammalian cardiomyocytes. The aims of this study were:

1. to validate a novel method utilising the IonOptix video edge-detection system for the continuous monitoring of cell width as an index of cell volume;
2. to establish whether freshly isolated mouse ventricular myocytes can activate an RVD in response to hypo-osmotic superfusion;
3. to compare the response of freshly isolated and cultured adult mouse ventricular myocytes to hypo-osmotic-induced cell swelling.

Male C57Bl/6 mice were anaesthetized (sodium pentobarbitone, i.p. 200 mg/kg with sodium heparin, 200 IU/kg), and the hearts excised and Langendorff perfused. Cardiomyocytes were isolated through enzymatic dispersion with collagenase (0.34 mg/ml) and trypsin (0.14 mg/ml) and directly pipetted onto glass cover slips in the superfusion chamber. Cardiomyocytes were superfused (1.5 ml/min, 37˚C) with an isosmotic, low Na solution supplemented with mannitol (~309 mOsmol/l) for 5 mins, then switched to a hypo-osmotic, low Na solution (no mannitol, ~217 mOsmol/l) for a further 10 mins. Changes in cell dimensions were measured simultaneously with both manual two-dimensional (2D) tracings of video images (length, width, area, 1 min intervals) and video edge detection (width only). A similar hypo-osmotic stress was subsequently used to compare RVD in freshly isolated and cultured cardiomyocytes (24hr culture on laminin-coated cover-slips).

2D tracings of hypo-osmotic-induced swelling in freshly isolated cardiomyocytes revealed substantial increases in cell width (111.3 ± 0.8% of pre-hypo-osmotic basal width at 10 min, $n = 5$) and area (111.5 ± 1.0%, $n = 5$), but not length (99.4 ± 0.4%, $n = 5$), with *no* evidence of RVD. Comparison of cell width measurements between the 2D tracings and the video-edge detection recordings showed a linear relationship. Further studies in freshly isolated and cultured cardiomyocytes identified occurrence of RVD in 2 out of 7 cultured cardiomyocytes, and complete absence of RVD in freshly isolated cells ($n = 7$).

These studies validate the use of the IonOptix video edge-detection system as a simple, continuous method for measuring small changes in cardiomyocyte width, as an index of cell volume. Freshly isolated mouse ventricular myocytes do not show any evidence of RVD in response to hypo-osmotic superfusion while cultured cells showed a limited response. Assuming cardiac myocytes *in vivo* are capable of mounting an RVD, this suggests the enzymatic isolation process perturbs the myocyte's ability to mount an RVD *in vitro* and this may be partially restored by short-term culture.

Expression of TRPC4 and desmonplakin in mouse hearts

Y. Chu, D.G. Allen and Y-K. Ju, Displine of Physiology, School of Medical Science, University of Sydney, NSW 2006, Australia.

The stretch-activated channels (SACs) are non-selective cation channels that respond to mechanical stress with an increase in open probability (Guharay & Sachs, 1984). Studies have shown that TRPC1 forms a stretch-activated cation channel in vertebrate cells (Maroto *et al.*, 2005). In our previous study, TRPC4 which is a closely related subgroup to TRPC1 (Schaefer, 2005), displayed a punctate labelling pattern in the plasma membranes and at cell termini (Ju *et al.*, 2007). Further Cx43-positive ($Cx43^+$) gap junctions were observed in the cardiomyocytes in mouse sinoatrial node (SAN) (Ju *et al.*, 2007). In this study, we further characterised the expression and distribution of TRPC4 and desmonplakin (DP), a necessary component of desmosomes in mouse hearts.

Single cardiomyocytes were enzymatically isolated from SAN region of mouse hearts. SANs were kept in KB solution for at least 4h at 4°C, before being triturated gently to dissociate the cells. The cells were then placed onto glass coverslips and maintained at room temperature for 1h to allow cells to adhere to the glass. Isolated single cardiomyocytes were then fixed in 4% paraformaldehyde for 1 min. They were permeabilised by incubating for 5 min in phosphate-buffered saline (PBS) containing 2% normal goat serum (NGS), 1% bovine serum albumin (BSA) and 0.1%Triton X-100. After blocking of nonspecific binding sites by incubation for 30 min with 0.01%BSA in PBS containing 10% NGS, single cardiomyocytes were exposed to primary antibodies. In order to determine the localisation of TRPC4 in cardiac myocytes, we double labelled for 1) TRPC4 and Cx43; and 2) TRPC4 and DP. In single cardiomyocytes, $Cx43^+$ gap junctions were detected in the plasma membrane and at cell termini, overlapping as well as non-overlapping but juxtaposed areas of Cx43 and TRPC4 were frequently seen, and suggesting Cx43 and TRPC4 were closely associated at the intercalated disc. DP^+ desmosomes were prominently detected at cell termini and in the plasma membrane. TRPC4 and DP were often juxtaposed at the intercalated discs.

Arrhymogenic right ventricular cardiomyopathy (ARVC) is a disease of desmosomes. Several studies have identified that mutations in genes that encode key components of the desmosome such as DP are responsible for ARVC (Dokuparti *et al.*, 2005; Sen-Chowdhry *et al.*, 2005). Our results have suggested that the specific localisation of TRPC4 imply that TRPC4 may form SACs in the region of cell connections in mouse hearts. We are currently working on different animal models to explore the possible implication of TRPC4 in cardiomyopathy.

Guharay F & Sachs F. (1984) *Journal of Physiology*, **352:** 685-701.

Maroto R, Raso A, Wood TG, Kurosky A, Martinac B & Hamill OP. (2005) *Nature Cell Biology*, **7:** 179-85.

Schaefer M. (2005) *Pflüger Archiv (European Journal of Physiology)*, **451:** 35-42.

Ju YK, Chu Y, Chaulet H, Lai D, Gervasio OL, Graham RM, Cannell MB & Allen DG. (2007) *Circulation Research*, **100:** 1605-14.

Dokuparti MVN, Pamuru PR, Thakkar B, Tanjore RR & Nallari P. (2005) *Journal of Human Genetics*, **50:** 375-81.

Sen-Chowdhry S, Syrris P & McKenna WJ. (2005) *Journal of Cardiovascular Electrophysiology*, **16:** 927-35.

Cellular mechanisms of STZ-induced diabetic cardiomyopathy

M-L. Ward,[1] L. Zhang,[1,2] A.R.J. Phillips[2,4,5] and G.J.S. Cooper,[2,3,5] [1]Department of Physiology, School of Medical Sciences, University of Auckland, Private Bag 92019, Auckland 1023, New Zealand., [2]School of Biological Sciences, University of Auckland, Private Bag 92019, Auckland 1023, New Zealand., [3]Department of Medicine, FMHS, University of Auckland, Private Bag 92019, Auckland 1023, New Zealand., [4]Department of Surgery, FMHS, University of Auckland, Private Bag 92019, Auckland 1023, New Zealand. and [5]Protemix Corporation, Auckland, New Zealand..

Sustained diabetes mellitus leads to a deterioration of heart function, which occurs independently of the macro- and micro-vascular diseases. In humans, development of diabetic cardiomyopathy is associated with increased risk of heart failure, but our understanding of the cellular mechanisms underlying diabetic cardiomyopathy remain unclear. Myocardial Ca^{2+} homeostasis has been reported to be altered during diabetes, and is believed to be involved in the diabetes-induced primary cardiomyopathy (Dhalla *et al.*, 1982). As well, extracellular matrix changes have also been implicated (Cooper *et al.*, 2004). The aim of this study was to investigate Ca^{2+} homeostasis, myocardial contractility, and extracellular matrix remodeling in an animal model of diabetes, in order to gain insights into the mechanisms underlying diabetic heart disease.

ECG measurements from anaesthetized animals (halothane, flow rate 2 ml/min with 100% O_2) immediately prior to euthanasia and dissection of trabeculae showed that the normalized QT interval was prolonged in diabetic rats (STZ: 0.192 ± 0.004 s, (n = 18); Control: 0.177 ± 0.004 s, (n = 11)), as was action potential duration (AP_{90}) recorded from the LV free-wall of isolated, perfused, hearts (STZ: 0.195 ± 0.009 s (n = 7); Control: 0.136 ± 0.010 s (n = 6)). Simultaneous measurements were made of isometric force and intracellular calcium ($[Ca^{2+}]_i$, as the ratio of fura-2/AM fluorescence), in left-ventricular trabeculae from STZ, and their age-matched Controls under physiological conditions (37 °C, 5 Hz and pH 7.4). STZ-induced diabetic rats, 8 weeks post injection, had depressed cardiac contractility. Peak systolic stress was decreased in STZ (STZ: 10 ± 1 mN mm^{-2}; Control: 17 ± 2 mN mm^{-2}, n = 7 in each group), with slower time to peak stress (STZ: 77 ± 3 ms; Control: 67 ± 7 ms) and time to 90% relaxation of stress (STZ: 76 ± 7 ms; Control: 56 ± 3 ms). Histological studies of fixed LV free wall showed that the structure of the thin myofilament (f-actin) was disrupted in diabetic hearts, and the content reduced. Despite the obvious contractile dysfunction, no discernable difference was found in the amplitude of the Ca^{2+} transient in diabetic rats, although the time constant of Ca^{2+} transient decay was slower (STZ: 61 ± 3 ms; Control: 49 ± 3 ms). Western blot analysis of SERCA2a and Na^+/Ca^{2+} exchanger expression was carried out in LV tissue from 8 week post-injection animals. It was found that SERCA2a expression was reduced in diabetic hearts, without significant changes of Na^+/Ca^{2+} exchanger expression. SERCA2a is the major Ca^{2+} transport protein responsible for rapid removal of cytosolic Ca^{2+}, thereby allowing relaxation to occur.

In conclusion, both prolonged action potential duration, and decreased expression of SERCA2a can explain the slower kinetics of the Ca^{2+} transient in diabetic rats, whereas the reduced contractility is more likely to be associated with the changes in f-actin content and structure.

Dhalla, NS, Pierce GN, Panagia V, Singal PK, & Beamish RE. (1982) *Basic Research in Cardiology*, **77:** 117-139.

Cooper GJ, Phillips AR, Choong SY, Leonard BL, Crossman DJ, Brunton DH, Saafi L, Dissanayake AM, Cowan BR, Young AA, Occleshaw CJ, Chan YK, Leahy FE, Keogh GF, Gamble GD, Allen GR, Pope AJ, Boyd PD, Poppitt SD, Borg TK, Doughty RN & Baker JR. (2004) *Diabetes* **53:** 2501-2508.

This study was approved by the University of Auckland Animal Ethics Committee, and supported by Health Research Council of New Zealand, and Protemix Corporation.

Structural studies of the phosphorylation domain of cardiac myosin binding protein-C

J. Hwang,[1] C.E. Oakley,[2] M. Kekic,[1] L.J. Brown[3] and B.D. Hambly,[1] [1]Pathology and Bosch Institute, University of Sydney, NSW 2006, Australia, [2]Molecular Biophysics, Florida State University, Tallahassee, Florida, USA and [3]Chemistry and Biomolecular Sciences, Macquarie University, NSW 2109, Australia.

Cardiac myosin binding protein–C (cMyBPC) is a large regulatory protein within the sarcomere, although the molecular mechanism underlying regulation is poorly understood. cMyBPC phosphorylation increases systolic tension, and dissociates the N-terminal region of cMyBPC from the S2 neck region of myosin. cMyBPC mutations are associated with familial hypertrophic cardiomyopathy (FHC), which is one of the most common forms of congenital heart disease. The N-terminal region of cMyBP-C that is phosphorylated and interacts with myosin S2 is the "linker" region between immunoglobulin (IgI) motifs C1 and C2 (C1-linker-C2). Unfortunately, the structure of C1-linker-C2 is unknown. *Ab initio* modeling of this fragment suggested the presence of alpha-helix. We hypothesize that the helix is located within the phosphorylatable linker region. Thus, we have cloned, expressed and purified several fragments of the N-terminal region of cMyBPC and performed structural analysis using circular dichroism (CD) spectroscopy. Our CD data obtained using smaller fragments of C1C2, namely, C1-linker and linker-C2, have confirmed the presence of a similar quantity of α-helix in both C1-linker and linker-C2. We therefore conclude that the α-helix is present in the linker region. Furthermore, we conclude that the folding of the α-helices within the linker region is likely to be independent of the adjacent IgI motifs, C1 and C2.

Electrophysiological properties of the *hERG* mutation E444K, found in familial atrial fibrillation

S.A. Mann,[1] J.A. Bursill,[1] T. Marciniec,[1] G. Guo,[2] R. Otway,[2] D. Fatkin[2] and J.I. Vandenberg,[1]
[1]Electrophysiology and Biophysics Programm, Victor Chang Cardiac Research Institute, Level 9, 384 Victoria Street, Darlinghurst, NSW 2010, Australia and [2]Molecular Cardiology Program, Victor Chang Cardiac Research Institute, Level 6, 384 Victoria Street, Darlinghurst, NSW 2010, Australia.

Atrial fibrillation (AF) is a cardiac arrhythmia characterized by rapid and irregular activation of the atria. Until recently, AF was regarded as a sporadic, non-genetic disorder. Although there is now accumulating evidence that familial aggregation of AF occurs in a significant proportion of cases, the extent to which genetic factors are responsible for this familial aggregation is unknown. Identification of single gene mutations in families will provide a framework for elucidation of key molecular and cellular pathways that underlie the more commonly-occurring complex forms of AF. Here we present a novel mutation in hERG (E444K), found in a case of familial AF, and the electrophysiological changes of the mutant channels compared to wildtype (WT) channels. Mutant channels were expressed in transiently transfected Chinese hamster ovary (CHO) cells. Whole-cell voltage-clamp recordings were performed in physiological solutions at room temperature. Under these baseline conditions the steady state half activation voltage of E444K channels was not significantly shifted compared to WT channels, whereas the steady state half inactivation voltage was shifted 10 mV in a hyperpolarizing direction compared to WT channels. Rates of activation, deactivation, and inactivation were not significantly altered compared to WT channels. Due to the left shifted steady state inactivation curve, at a given membrane potential the fraction of inactivated mutant channels will be greater than the fraction of inactivated WT channels at the same potential, ultimately leading to a smaller potassium current through hERG channels at the end of the cardiac action potential. To further assess the effects of the mutated channel on cardiac action potential, E444K transfected CHO cells were voltage-clamped to prerecorded human atrial action potential waveforms for both a normal sinus rhythm as well as an episode of atrial fibrillation. During the AF episode an increase in potassium current was observed in E444K experiments as well as in WT control experiments, with no significant difference between mutant and WT channels. We conclude that at baseline conditions the effect of the E444K mutation is not sufficient to change atrial action potential shapes sufficiently to promote AF.

Preparation of PCR-grade RNA from myocardial biopsy tissue of cardiac surgery patients

W.T.K. Ip,[1,2] L.M.D. Delbridge[1] and S. Pepe,[2] [1]Cardiac Phenomics Laboratory, Department of Physiology, University of Melbourne, Parkville, VIC 3010, Australia and [2]Department of Surgery, Alfred Hospital, Faculty of Medicine, Nursing and Health Sciences, Prahran, VIC 3181, Australia.

Intact RNA is a key element for the generation of meaningful and reproducible gene expression analysis from real-time PCR. This is especially important for experiments that involve human tissues which are often available in limited supply. The aims of this study are to determine the optimal RNA extraction process for human atrial tissues and to investigate the effects of prolonged tissue storage on real-time PCR gene amplification. Human atrial appendages from patients undergoing coronary artery bypass surgery were pulverized on liquid nitrogen using mortar and pestle and divided into 2 sets of 100 mg aliquots to allow parallel comparison of the RNA preparation obtained using 1) commercial silica-gel membrane based RNA extraction kits (RNeasy Fibrous Tissue Midi kit, Qiagen), which contains an on-column proteinase-k and DNase treatment as part of the protocol, and 2) the 'sequential extraction protocol' where RNA were isolated using a guanidium thiocyanate based cell lysis buffer (TRIzol Reagent, Invitrogen) followed by DNase treatment (Deoxyribonuclease I - amplification grade, Invitrogen) and clean-up (MinElute Cleanup kit, Qiagen). Comparison of the RNA preparations extracted using the two methods have revealed that the sequentially extracted preparations exhibited higher RNA integrity (28S/18S ratio = 2.91 ± 0.31 *vs.* 1.44 ± 0.10, for sequential and kit preparations respectively, $p < 0.001$) and increased RNA purity (RNA Integrity Number, RIN = 9.25 ± 0.19 *vs.* 7.60 ± 0.46, for sequential and kit preparations respectively, $p = 0.009$). Protein contamination was found to be low in both groups (A260/280 ratio = 1.93 ± 0.2 and 1.75 ± 0.1, $p = 0.409$). Investigation of how these RNA measurements are translated to efficient gene amplification were undertaken by performing real-time PCR to assess gene amplification of 18S and GAPDH (two genes that are of rRNA and mRNA origin) in the samples that were extracted using the sequential and kit methods. Despite the variation in RNA integrity and purity, all RNA preparations were found to amplify 18S and GAPDH with similar efficiencies regardless of RNA extraction method (18S amplification efficiency: 1.41 ± 0.04 and 1.47 ± 0.05 for sequential and kit extraction respectively, $p = 0.391$; GAPDH amplification efficiency: 1.86 ± 0.01 and 1.86 ± 0.02 for sequential and kit extraction respectively, $p = 0.577$). All PCR reactions were carried out under pre-established optimized PCR conditions.

The second aim of this study was to investigate the effects of prolonged tissue storage on RNA integrity and real-time PCR gene amplification. RNA was extracted from human atrial appendages, stored at -80ºC for 1 and 5 years designated as 'recent' and 'archived' samples respectively. Similar RNA measurements and gene amplification measurements as described above were assessed. RNA recovery was not different between the archived and recent samples (71.00 ± 10.15 ng/µl *vs.* 74.80 ± 12.95 ng/µl, $p = 0.846$). No differences were found in the RNA integrity measurements including the RIN (8.53 ± 0.07 and 7.04 ± 0.43, for archived and recent samples, $p = 0.124$) and 28S/18S ratio (1.53 ± 0.13 and 1.38 ± 0.14, for archived and recent samples, $p = 0.500$), suggesting similar sample purity and integrity between these sample groups. Real-time PCR was used to assess gene amplification of 18S and GAPDH in the recent and archived samples. All samples were found to exhibit similar amplification efficiency regardless of tissue storage period (18S amplification efficiency: 1.44 ± 0.1 and 1.48 ± 0.05 for archived and recent samples, $p = 0.740$; GAPDH amplification efficiency: 1.85 ± 0.2 and 1.86 ± 0.1 for archived and recent samples, $p = 0.450$).

The present study has established a stringent sample-handling protocol to optimize human gene expression outcomes in human myocardial specimens. Samples extracted using the conventional guanidium thiocyanate based lysis buffer followed by DNase treatment and clean-up have been found to be a better extraction compared to the commercially available silica-gel-membrane based extraction columns. These findings suggest that if simultaneous RNA and protein extraction by TRIzol reagent is desired, extraction of RNA by the sequential method could achieve outcomes that are even better than those achieved by the commercial silica-gel-membrane based RNA extraction kits. In addition, we have found that human atrial tissue samples that have been stored in -80ºC for up to 5 years are suitable for PCR gene expression study.

Protein trafficking defects as a cause of congenital long QT syndrome

J.T. Zhao,[1] J. Skinner,[2] A.P. Hill[1] and J.I. Vandenberg,[1] [1]Mark Cowley Lidwill Research Program in Cardiac Electrophysiology, Division of Molecular Cardiology and Biophysics, Victor Chang Cardiac Research Institute, NSW 2010, Australia and [2]Paediatric and Congenital Cardiac Services, Auckland City Hospital Level 3, Building 32, Private Bag 92 189, Auckland 1030, New Zealand.

Congenital long QT syndrome (LQTS) is a disease characterized by prolongation of QT intervals on the electrocardiogram (ECG), syncope and life-threatening arrhythmias. The chromosome 7-linked form, LQT2, is caused by mutations in the human ether-a-go-go-related gene (HERG). In the present study, we are investigating mutations that cause trafficking defects, which account for 80% of all LQT2 cases. In particular we wish to investigate whether the severity of the clinical phenotype is proportional to the extent to which trafficking defective mutant channels exert a dominant negative effect on trafficking of wild-type alleles. A Western blot assay has been established to characterize the trafficking properties WT and mutant HERG channels expressed in HEK293 cells. The G572S mutation results in proteins that are retained in the ER and co-expression of G572S and WT channels results in the WT channel also being largely retained in the ER. Patch clamp assays showed that co-expression of WT and G572S resulted in a >90% suppression of functional channel expression. Immuno-fluorescence assays to further investigate the co-localization of WT and mutant channels will be performed. However, the results to date already indicate that the G572S mutant has a significant dominant effect that is consistent with the severe clinical phenotype seen in patients with this mutation. Further, this study illustrates the power of *in vitro* studies to help establish genotype-phenotype relationships in LQT2 and this could have significant clinical impact on the management of this disorder.

Dynamics of inactivation of hERG potassium channels

P. Ju, A.P. Hill, T. Marciniec and J.I. Vandenberg, Mark Cowley Lidwill Cardiac Electrophysiology and Biophysics Program, Victor Chang Cardiac Research Institute, Sydney, NSW 2010, Australia.

Potassium ion channels encoded by the human ether-a-go-go-related gene (hERG) have very unusual kinetic behavior, characterized by slow activation but very rapid inactivation. The unusually rapid and voltage-dependent inactivation of hERG is crucial for normal cardiac repolarization and suppression of propagation of premature beats. Inactivation of hERG channels result from conformational changes in the outer pore domain of the channel, however, the characteristics of the paths connecting the open conformation and inactive conformation of the channel remain largely unexplored. The aim of this study was to reveal the structural and temporal sequence of domain motions during hERG inactivation using the technique of rate-equilibrium linear free energy relationship (REFER, or phi-value) analysis. Wild type or mutant hERG cRNA was injected into *Xenopus laevis* oocytes and currents recorded using two electrode voltage clamp techniques. Rates of inactivation and recovery from inactivation were analysed at voltages in the range from −200 mV to +80 mV (the precise voltage range varied for each mutant) by fitting single exponential functions to the current traces recorded during double or triple pulse protocols. From these data we interpolated a value for the forward and reverse rate constants as well as the equilibrium constant for inactivation at 0 mV. The phi-value for each mutant was calculated as the ratio of the change in the log of the forward rate constant versus the change in the log of the equilibrium constant. Mutations in the S4, S5P and S5 domains all give phi-values of ~0.6, suggesting that mutations to these domains perturb early steps in the open to inactive state transition. In contrast, mutations to S631 have phi values of ~0.3, so mutations to S631 perturb a later step in the open-inactive state transition. Lastly, mutation to S624 gives a phi value of 0.01, so it clearly perturbs a very late step in the open-inactive state transition. These data suggests that inactivation involves a conformational wave of domain motions with peripheral domains moving earlier than more proximal domains and the final transition occurring at the interacellular end of the selectivity filter.

The measurement of inactivation in the human ether-á-go-go related gene channel

M.J. Perrin,[1,2] T.J. Campbell[2] and J.I. Vandenberg,[1] [1]Victor Chang Cardiac Research Institute, 384 Victoria Street, Darlinghurst, NSW, 2010, Australia and [2]St Vincent's Clinical School, Level 5 DeLacey Building, St Vincent's Hospital, Victoria Street, Darlinghurst, NSW 2010, Australia.

The human ether-á-go-go related gene (hERG) encodes the α-subunit of the rapid delayed rectifier K^+ channel (IK_r) in the heart. IK_r displays marked inward rectification due to a very fast rate of channel inactivation at positive membrane potentials. The correct measurement of inactivation is of fundamental importance in the characterisation of any hERG mutation. We hypothesised that the standard method for measuring inactivation - a 3 pulse voltage clamp protocol - was flawed giving a Boltzmann distribution of steady-state inactivation (SSinact) left-shifted compared to the true value. To test this hypothesis, whole cell patch-clamping was performed on CHO-K1 cells stably expressing wild-type hERG. Standard 3 and 2 pulse voltage clamp protocols were employed and analysed. A virtual model of hERG gating was used to assess the reliability of the experimental data. The SSinact of hERG measured with a 3 pulse protocol was significantly left shifted compared with a 2 pulse protocol. V0.5 for 3 pulse: -90.6mV +/- 3.3mV. V0.5 for 2 pulse: -74.6mV +/- 3.3mV, (p = 0.04). Virtual modelling confirmed the validity of these findings and provided evidence that the 2 pulse protocol was a better representation of the true distribution. The standard 3 pulse voltage protocol to measure SSinact results in a SSinact curve left-shifted compared to a 2 pulse protocol. Theory and virtual modelling evidence suggests greater accuracy with a 2 pulse protocol. Almost all papers published to date on hERG inactivation utilise a 3 pulse voltage clamp protocol. There is now evidence that published values of steady-state inactivation in hERG differ significantly from the true value.

Evidence for functional coupling between the mitochondria and the L-type calcium channel in the heart

H.M. Viola, P.G. Arthur and L.C. Hool, Cardiovascular Electrophysiology Laboratory, School of Biomedical, Biomolecular and Chemical Sciences, M311, Physiology, The University of Western Australia, Crawley, WA 6009, Australia.

Transient exposure of ventricular myocytes to hydrogen peroxide leads to an increase in L-type calcium channel basal current and increased superoxide production by the mitochondria. Activation of the channel with the dihydropyridine receptor agonist Bay K(-) mimics this response. Enhanced superoxide production occurs with enhanced calcium uptake into the mitochondria. However, superoxide is also produced when the mitochondrial membrane potential is increased. We examined the relationship between activation of the L-type calcium channel and regulation of the mitochondrial membrane potential. Ventricular myocytes were isolated from hearts excised from anesthetised guinea-pigs. Activation of the L-type calcium channel with Bay K(-) or 45 mM KCl caused a modest but statistically significant increase in mitochondrial membrane potential assessed with the fluorescent indicator JC-1. The increase in membrane potential occurred in the absence of extracellular calcium and presence of the Na/H exchanger inhibitor amiloride and Na^+ channel inhibitor tetrodotoxin. In addition Ru360, an inhibitor of the mitochondrial calcium uniporter did not prevent the increase in mitochondrial membrane potential induced by 45 mM KCl. Regulation of channel activation is mediated through the auxiliary β subunit that is also tethered to the cytoskeleton. Depolymerisation of F actin with latrunculin A prevented the increase in mitochondrial membrane potential by 45 mM KCl but did not affect the increase in superoxide production by the mitochondria induced by 1 mM caffeine. We conclude that the L-type calcium channel can regulate mitochondrial function. A functional coupling of the channel with the mitochondria may assist with regulating ATP production on a beat to beat basis.

The effect of high hydrostatic pressure and TMAO on gating of MscS of *E. coli*

E. Petrov, P.R. Rohde and B. Martinac, School of Biomedical Sciences, The University of Queensland, St Lucia, QLD 4072, Australia.

The activity of MscS, the bacterial mechanosensitive ion channel of small conductance, has been investigated under high hydrostatic pressure (HHP) using a "flying-patch" patch-clamp technique. In inside-out excised patches of giant spheroplasts of *E. coli*, MscS was activated by negative pipette voltage to allow for open probability measurement at different levels of HHP up to 90 MPa. MscS open probability was found to gradually decrease on increasing HHP. To determine the extent that the cytoplasmic and transmembrane domains of the channel may contribute to this effect, the osmolyte methylamine N-oxide (TMAO) was applied to the cytoplasmic side of the excised spheroplast membrane patches. In the presence of TMAO the inhibitory effect of HHP on MscS activity was suppressed at pressures of up to 50 MPa. Above 50 MPa, channel open probability decreased similarly in absence or in presence of TMAO indicating that at pressures higher than 50 MPa, TMAO at concentrations used in this study could not counteract the effect of HHP on the MscS channel activity. The change in the reaction volume calculated in the presence of TMAO differs significantly from the reaction volume calculated in absence of TMAO. Our study suggests that TMAO can stabilize the open state of the MscS channel at HHP, most likely by interacting with the cytoplasmic domain of MscS.

Supported by the Australian Research Council.

Rapid incorporation of bacterial mechanosensitive ion channel proteins MscL and MscS into liposomes using a modified sucrose method

A.R. Battle, E. Petrov, P. Pal and B. Martinac, Department of Physiology and Pharmacology, School of Biomedical Sciences, The University of Queensland, St Lucia 4072, Australia.

Bacterial mechanosensitive (MS) ion channels act as emergency relief valves in order to help bacterial cells to survive sudden changes in external osmolarity due to hypo-osmotic shock (Martinac, 2004; Perozo, 2006). Traditional methods of incorporating MS channels into liposomes have been successful for the MscL, the MS channel of large conductance, but not for MscS, the MS channel of small conductance. Here we present a novel time efficient procedure for the successful incorporation of either of these proteins into artificial liposomes. This method is based on preparing giant liposomes using sucrose (Di Maio *et al.*, 2006; Akashi *et al.*, 1996) and subsequently adding purified MscL or MscS protein to the liposomes suspended in the sucrose solution. Electrophysiological recordings of both liposome preparations reveal patches with multiple channels which are activated by increasing membrane tension.

Martinac B. (2004) *Journal of Cell Science*, **117:** 2449-60.

Perozo, E. (2006) *Nature Reviews. Molecular Cell Biology*, **7:** 109-19.

Di Maio IL, Carl D, Langehanenberg P, Valenzuela SM, Battle AR, Al Khazaaly S, Killingsworth M, Kemper B, von Bally G & Martin DK. (2006) *Proceedings of SPIE-The International Society for Optical Engineering (BioMEMS and Nanotechnology II)*, **6036:** 60361R1-60361R9.

Akashi K, Miyata H, Itoh H & Kinosita K Jr. (1996) *Biophysical Journal*, **71:** 3242-50.

Supported by the NH&MRC.

Are α9α10 nicotinic acetylcholine receptors a pain target?

S.T. Nevin,[1] R.J. Clark,[2] H. Klimis,[3] M.J. Christie,[3] D.J. Craik[2] and D.J. Adams,[1] [1]School of Biomedical Sciences, The University of Queensland, Brisbane, QLD 4072, Australia, [2]Institute for Molecular Bioscience, The University of Queensland, Brisbane, QLD 4072, Australia and [3]Pain Management Research Institute, Kolling Institute, University of Sydney at Royal North Shore Hospital, St Leonards, NSW 2065, Australia.

The synthetic α-conotoxin Vc1.1 (ACV1) is a small disulfide bonded peptide currently in development as a treatment for neuropathic pain. Unlike Vc1.1, the native post-translationally-modified peptide vc1a does not act as an analgesic *in vivo* in rat models of neuropathic pain. Recently, it has been proposed that the primary target of Vc1.1 is the α9α10 nicotinic acetylcholine receptor (nAChR) (Vincler & McIntosh, 2006). The aim of the present study was to examine the potency and efficacy of the post-translationally modified analogues vc1a, [P6O]Vc1.1 and [E14γ]Vc1.1 at α9α10 nAChRs and in neuropathic pain studies, respectively.

Electrophysiological recordings from nAChRs exogenously expressed in *Xenopus* oocytes were as described previously . Membrane currents were recorded using an automated OpusXpress™ 6000A workstation. Acetylcholine (30 μM) was applied for 2 s with 400 s washout periods between applications. Conopeptides were bath applied and co-applied with the agonist. Cells were voltage clamped at –80 mV with peak current amplitudes measured before and following incubation of the peptide. Neuropathic pain was assessed using partial ligation of the left sciatic nerve (PNL) , with the effects of the conotoxins on withdrawal thresholds and motor function evaluated.

Vc1.1 has been shown previously to inhibit α3-containing nAChRs but only at micromolar concentrations and was inactive at concentrations up to 10 μM at α7, α4-containing and muscle (α1β1γδ) nAChRs expressed in oocytes (Clark *et al.*, 2006). Vc1.1 inhibited reversibly α9α10 nAChR-mediated currents in a concentration-dependent manner with an IC_{50} of 64.2 ± 15.0 nM (n = 12). Application of vc1a, [P6O]Vc1.1 and [E14γ]Vc1.1 also inhibited reversibly α9α10 nAChRs in a concentration-dependent manner, giving IC_{50}'s of 62.9 ± 5.2 nM, 99.1 ± 29.7 nM, 65.3 ± 14.9 nM (n = 10-12), respectively.

PNL produced a profound reduction in paw withdrawal threshold from a pre-surgery baseline of 12.9 ± 0.7 g to 0.7 ± 0.1 g (n = 33) 12-16 days after surgery. As reported previously (Satkunanathan *et al.*, 2005), intramuscular injection of 60 μg Vc1.1 produced significant partial reversal of allodynia associated with nerve injury. By contrast, 60 μg/rat injections of vc1a or [P6O]Vc1.1 had no significant effect on mechanical allodynia.

We demonstrate here that Vc1.1 is approximately 100-fold more potent for α9α10 nAChRs, and produces a significant partial reversal of allodynia associated with nerve injury. Similarly, the post-translationally modified peptides vc1a, [P6O]Vc1.1 and [E14γ]Vc1.1 inhibit α9α10 nAChRs with equivalent potencies to Vc1.1 and had no effect on mechanical allodynia in a nerve injury model of neuropathic pain. The lack of activity of vc1a on these nAChR subtypes is consistent with findings reported previously in bovine chromaffin cells and other rat models of neuropathic pain , however, vc1a is equally potent with Vc1.1 as an antagonist of α9α10 nAChRs. Synthetic vc1a and the partially modified homologues [P6O]Vc1.1 and [E14γ]Vc1.1 are all active at α9α10 nAChRs, but not at any of the other nAChR subtypes. However, given that Vc1.1, but not vc1a nor its analogue [P6O]Vc1.1, were able to inhibit a vascular response to pain and reduce chronic pain in several animal models of human neuropathy it is highly unlikely that the molecular mechanism or the therapeutic target for the treatment of neuropathic pain is *via* a α9α10 nAChR.

Clark RJ, Fischer H, Nevin ST, Adams DJ & Craik DJ. (2006) *Journal of Biological Chemistry* , **281:** 23254-63.
Satkunanathan N, Livett B, Gayler K, Sandall D, Down J & Khalil Z. (2005) *Brain Research*, **1059**:149-58.
Vincler M & McIntosh JM. (2007) *Expert Opinion on Therapeutic Targets* **11:** 891-7.

FRET-ing over CLIC1 insertion into the membrane

S.C. Goodchild,[1] P.M.G. Curmi[2] and L.J. Brown,[1] [1]Department of Chemistry and Biomolecular Sciences, Macquarie University, Sydney, NSW 2109, Australia and [2]School of Physics, The University of New South Wales, Sydney, NSW 2052, Australia.

Conventionally, it has been thought that proteins adopt a well defined tertiary structure. However, it is increasingly becoming apparent that some proteins can exist in at least two or more stable conformations. A striking feature of the recently described CLIC (chloride intracellular channel) protein family is that they can exist in both soluble and integral membrane forms. The crystal structures of soluble monomeric and non-covalent dimeric CLIC1 have been solved. The monomer structure showed that the CLICs are structurally homologous to the glutathione S-transferase (GST) superfamily. However, unlike other GST proteins CLICs can traverse the membrane and display ion channel activity. Soluble CLIC1 has been demonstrated to insert into the lipid bilayer to form an active channel in the absence of other cellular protein. This change of conformation must involve large-scale structural rearrangements to confer favourable interactions with the membrane by exposing hydrophobic residues. However, the manner by which CLICs insert into the bilayer and the factors controlling this process remain unclear.

In this study, fluorescence resonance energy transfer (FRET) was used to monitor the insertion of CLIC1 into the membrane. The distance between a single native tryptophan located in the putative transmembrane membrane region of the N-domain (Trp-35) and four native cysteine residues of the C-domain individually modified with the fluorescent label 1,5-IAEDANS, were measured in the presence and absence of lipid. Upon interaction with the bilayer, the distance between Trp-35 and Cys-223 increased significantly suggesting an unfolding between the C-domain and N-domain as the N-domain is inserted into the membrane. This result demonstrates that CLIC1 indeed undergoes a large conformational change upon interaction with the membrane, reinforcing the notion of the CLIC family of proteins as dynamic entities and in turn, challenging many accepted views of protein structure and ion channel biochemistry.

Chloride conductance in the transverse tubular system of rat skinned skeletal muscle fibres

T.L. Dutka, D.G. Stephenson and G.D. Lamb, Department of Zoology, La Trobe University, Melbourne, VIC 3086, Australia.

Contraction in skeletal muscle fibres is governed by excitation of the transverse-tubular (T-) system, but the properties of the T-system and their importance in normal excitability are not well defined. Here we investigate the properties of the T-system chloride conductance using rat skinned muscle fibres in which the sarcolemma has been mechanically removed but the normal excitation-contraction coupling mechanism kept functional. Male Long-Evans hooded rats were killed under deep anesthesia (2% v:v halothane) and both extensor digitorum longus (EDL) muscles were rapidly excised and pinned at resting length for 30 min at room temperature: one in an extracellular solution with Cl^- and the other without Cl^- (Cl^- containing solution (mM): NaCl (135), KCl (4), $CaCl_2$ (2.5), $MgCl_2$ (1), NaH_2PO_4 (0.3), HEPES (10), pH to 7.2 with NaOH; zero Cl^- solution (mM): Na-methylsulphate (130), K_2HDTA (hexamethylene-diamine-tetraacetic acid) (2), Ca-HDTA (2.5), Mg-HDTA (1), total $HDTA^{2-}$ (10), pH to 7.2 with NaOH; the osmolality and concentrations of each cation were nearly identical in these two solutions). In parallel experiments muscles were soaked in the aforementioned extracellular solutions with or without 100 nM phorbol 12, 13-dibutyrate present (made from a 100 μM stock in DMSO). Single fibres were mechanically-skinned alternately from both EDL muscles, connected to a force transducer and immersed in a standard K-HDTA solution (1mM free Mg^{2+}; 8 mM total ATP; 10 mM creatine phosphate at pH 7.10, containing 50 μM EGTA, pCa 7.0) with 0 or 3 mM Cl^- added to the bathing solution where appropriate. Where required, 100 μM 9-anthracene carboxylic acid, a chloride channel blocker, was added from a 100 mM stock made in DMSO, with the same volume of DMSO added to the matching control solutions. Additionally, a bathing solution with all Na^+ removed (to inhibit the Na^+/K^+-ATPases) was also made. Individual fibres were then electrically stimulated (0-125 V cm^{-1}, 1 ms pulse) to produce either twitch or tetanic (50 Hz, 75 V cm^{-1}) force responses (Posterino *et al*., 2000; Dutka & Lamb, 2007). When the T-system chloride conductance was eliminated, either by removal of all Cl^- or by block of the chloride channels with 100 μM 9 AC or by treating muscles with 100 nM phorbol 12,13-dibutyrate, there was a marked reduction in the threshold electric field intensity required to elicit a T-system action potential (AP) and twitch response. Calculations of the T-system chloride conductance indicated that it constitutes most of the total chloride conductance observed in intact fibres. Blocking the chloride conductance increased the size of the twitch response by approximately 14% (absolute force) and was indicative that Cl^- normally carries part of the repolarising current across the T-system membrane on each AP. Blocking the T-system chloride conductance also reduced peak tetanic force responses at higher frequency stimulation (100 Hz) and caused the tetanic force to fade considerably quicker, owing to rapid loss of T-system excitability during the AP train. Blocking activity of the Na^+/K^+-ATPases in the T-system membrane by removing all Na^+ from the bathing solution caused a loss of excitability owing to K^+ build-up in the sealed T-system, and this occurred approximately 4 times faster when the chloride conductance was absent. This study unequivocally demonstrates that the chloride conductance of the T-system plays a vital role in maintaining normal muscle excitability, reducing the accumulation of K^+ in the T-system and its depolarizing effect, and hence helping prevent the muscle fatigue that would otherwise readily ensue.

Dutka TL & Lamb GD. (2007) *American Journal of Physiology*, **292:** C2112-21.
Posterino GS, Lamb GD & Stephenson DG. (2000) *Journal of Physiology*, **527:** 131-7.

The RyR1 SPRY2 domain binds to the DHPR α1S II-III loop and to the RyR1 binding site for the DHPR β1a subunit

H-S. Tae, M.G. Casarotto, P.G. Board and A.F. Dulhunty, Division of Molecular Bioscience, The John Curtin School of Medical Research, Australian National University, ACT 2601, Australia.

Excitation-contraction coupling (ECC) links electrical signals in muscle fibers to the massive release of Ca^{2+} from the sarcoplasmic reticulum (SR) that initiates muscle contraction. A physical interaction between the dihydropyridine-sensitive L-type Ca^{2+} channel (DHPR) and the SR-Ca^{2+} release channel; ryanodine receptor 1 (RyR1) are prerequisites for skeletal muscle ECC. This protein-protein interaction depends on a cytoplasmic loop in the DHPR α1S subunit, between the second and third transmembrane domains (II-III loop), that allows the receptor to communicate allosterically with RyR1. Although it is generally accepted that the II-III loop is involved in the physical interaction between the DHPR and RyR1, the location of its binding site on RyR1 remains elusive. Skeletal ECC is also strongly dependent on residues in the variably spliced ASI region of RyR1 (Thr3471 – Gly3500), which bind to the β1a subunit of the DHPR. The ASI region (β1a binding region) has a sequence of positively charged residues that very similar in structure to those of α1S II-III loop. Leong & Maclennan (1998) co-immunoprecipitated 35S-labeled RyR1 fragments with the DHPR II-III loop and identified a stretch of 37-RyR1 amino acid residues that were involved in the interaction. Most of the identified residues are located within a region of RyR1 known as SPRY2 domain. Based on these observations, we proposed that the second of three RyR1-SPRY domains (SPRY2) is the interaction site for the II-III loop. SPRY domains were initially identified in a fungal protein (SplA) and in ryanodine receptor (RyR) (Rhodes *et al.*, 2005) and hence named SPRY. So far, the RyR1-SPRY domains have been classified as domains of an unknown function (Ponting *et al.*, 1997). Our aims were therefore (a) to characterise binding of the RyR1-SPRY2 domain to the II-III loop and identify key regions of the II-III loop that are involved in the interaction and (b) to determine whether the AS1 region also bound to SPRY2. In order to achieve these aims, we have used nuclear magnetic resonance (NMR) and spectrofluorimetry techniques with the SPR2 domain and the II-III loop, as well as mutations in both proteins to identify the key regions involved in the interactions. Experimental results demonstrated that SPRY2 domain binds at different binding affinity to two 'critical regions' (A and C) in the N-terminal and central regions (defined by El-Hayek *et al.*, 1995) of the II-III loop at non-analogous binding sites. The binding affinity for the A region is 8.3 ± 0.3 μM, while the affinity for the C region is 20.6 ± 0.4 μM. Mutational analysis showed that a negatively charged domain of SPRY2, including most of the 37 residues identified by Leong & Maclennan (1998), binds to the positively charged motif of the II-III loop-A region. We find that a peptide corresponding to the ASI region also interacts with the SPRY2 domain with an affinity of 1.4 ± 0.1 μM. We have provided compelling evidence that the RyR1-SPRY2 domain is a functional domain, which binds to the DHPR II-III loop and to the ASI domain of RyR1.

Leong P & Maclennan DH. (1998) *Journal of Biological Chemistry*, **273:** 7791-4.

Rhodes DA, de Bono B & Trowsdale J. (2005) *Immunology*, **116:** 411–7.

Ponting C, Schultz J & Bork P. (1997) *Trends in Biochemical Sciences*, **22:** 193–4.

El-Hayek & Ikemoto Wang J, Hamilton SL & Ikemoto N. (1995) *Journal of Biological Chemistry*, **270:** 22116-8.

Cheng W, Altafaj X, Ronjat M & Coronado R. (2005) *Proceedings of the National Academy of Science USA*, **102:** 19225-30.

Effects of calmodulin on protein synthesis in mechanically skinned skeletal muscle fibres of the rat

D.W. Jame, M. Jois and D.G. Stephenson, School of Life Sciences, La Trobe University, VIC 3086, Australia.

The rate of protein synthesis in mechanically skinned skeletal muscle fibres of the rat has been shown to depend markedly on the level of ionised Ca^{2+} present (Jame *et al.*, 2006). Protein synthesis was completely abolished when the [Ca^{2+}] was raised from 280 nM to 1 μM; however, the mechanism behind this is not known. Recent studies (Rose *et al.*, 2005) have revealed that during dynamic exercise a Ca^{2+}-calmodulin dependent process activates eukaryotic elongation factor2 (eEF2) kinase causing increased phosphorylation of eEF2 thereby decreasing its activity. This inhibits mRNA translation indicating that the depression in muscle protein synthesis during exercise is regulated by Ca^{2+}-calmodulin. As the skinned fibre preparation enables control over the intracellular environment, the aim of this study was to determine whether the Ca^{2+}-sensitive rate of protein synthesis was also calmodulin dependent.

Experiments were conducted using our novel technique in accordance with procedures described previously (Jame *et al.*, 2006). In brief, fibres were mechanically skinned from freshly dissected soleus muscles of rats (3-5 months old Long-Evans, hooded) killed by isoflurane overdose. The skinned fibre segments were then incubated at 30ºC for 2 hours in a medium mimicking the myoplasmic ionic environment and containing ^{3}H-leucine and a mixture of all the 20 amino-acids required for protein synthesis. Protein synthesis rates were measured as the cycloheximide-sensitive incorporation of ^{3}H-leucine in the presence and absence of 8 μM calmodulin in the incubation medium.

In media containing 280 nM Ca^{2+} strongly buffered with EGTA, the presence of 8 μM calmodulin markedly reduced the rate of protein synthesis. However, reducing the calmodulin concentration in the medium to 0.8 μM had no effect on the synthesis rate. There was also no significant difference between the rates of synthesis in the presence and absence of 8 μM calmodulin when the [Ca^{2+}] in the incubating media was less than 100 nM. These findings reveal that calmodulin does have an inhibitory action on protein synthesis in muscle and that this inhibition is dependent on the concentration of both calmodulin and Ca^{2+}. In conclusion, Ca^{2+}-calmodulin dependent processes play a critical role in the regulation of protein synthesis in skeletal muscle.

Jame DW, Jois M & Stephenson DG. (2006) *Proceedings of the Australian Physiological Society*, **37:** 62P.

Rose AJ, Broholm C, Kiillerich K, Finn SG, Proud CG, Rider MH, Richter EA & Kiens B. (2005) *Journal of Physiology*, **569:** 223-8.

This study was supported by an NH&MRC grant.

Contralateral strength gains following a 4-week progressive resistance exercise programme

J.A. Sampson, H. Groeller and G. Jacobs, School of Health Sciences, University of Wollongong, NSW 2522, Australia.

A recent meta-analysis observed a 7.8% pooled estimate increase on the maximal voluntary strength of the contralateral limb following unilateral training. Thirty untrained male subjects completed 4 weeks of resisted single dominant limb exercise progressively increasing in load 10% weekly commencing at 50% of 1 repetition maximum (1RM). Subjects were positioned supine and performed single limb dynamic contractions through 60°-160° of elbow flexion of the dominant limb. Strength was assessed isometrically *via* maximal voluntary contraction (MVC) at 90° and dynamically to determine 1RM. Surface electrodes (Ag/AgCL) recording electromyographic activity at the biceps brachii was low- (500Hz) and high- (10Hz) pass filtered (Digitimer, Neurolog NL144, NL135). Peak and average EMG was calculated from Root Mean Square (RMS) (spike 2 Ver5.13) over 250 ms windows with a 50% overlap. Data are presented as mean ± SEM (* denotes significant difference).

Test	Pre test	Post test	Change (%)
Trained limb 1RM (kg)	17.2 ±0.7	20.2 ±0.7	17.5 *
Contralateral 1RM (kg)	18.0 ±6.8	19.5 ±7.4	8.5 *
Trained limb MVC (Nm)	81.6 ±4.1	89.1 ±4.2	9.2 *
Contralateral MVC (Nm)	83.8 ±3.5	87.7 ±4.3	4.7

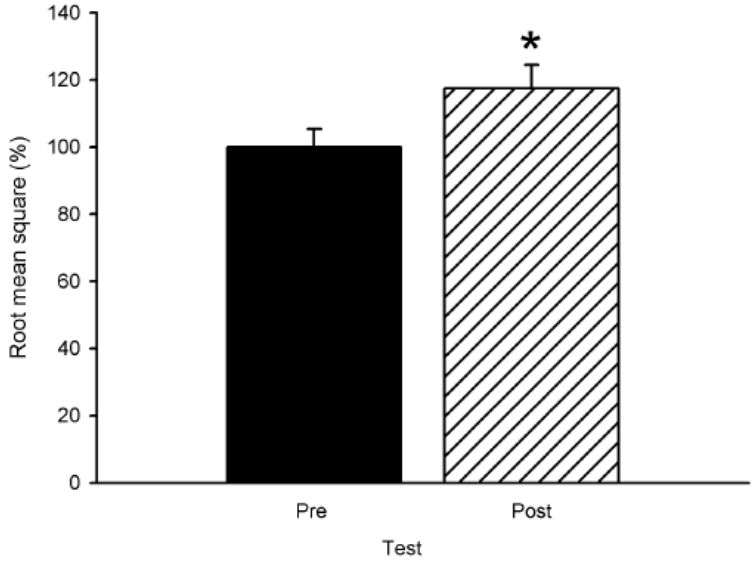

A significant increase in dynamic 1RM strength was observed in trained and contralateral limbs after training. A significant increase in exercise limb MVC and non-significant increase in contralateral limb MVC were observed (Table). Mean RMS significantly increased (p = 0.019) 13.7% during trained limb 1RM. Peak RMS significantly increased (p = 0.008) 15.9% during contralateral 1RM (figure). No significant differences were observed in isometric MVC EMG of the trained and contralateral limbs. Increased RMS and 1RM after resistance training suggests strength adaptations were achieved via neural mechanisms specific to the training mode.

Curve fitting model to quantify the rate and extent of force loss during different phases of fatigue in isolated skeletal muscle

S.P. Cairns[1] and D.S. Loiselle,[2] [1]School of Sport and Recreation, Faculty of Health and Environmental Sciences, AUT University, Private Bag 92006, Auckland 1020, New Zealand and [2]Department of Physiology, School of Medicine, University of Auckland, Auckland 92019, New Zealand.

Fatigue induced with repeated tetani is often quantified using a fatigue index (Burke *et al.*, 1973), *i.e.*, the peak force at a defined stimulation time relative to that of the first tetanus. However, this approach fails to reveal detail about the time-course of fatigue. It is also established that several phases of fatigue exist that reflect different underlying mechanisms (Lännegren & Westerblad, 1991); hence there is a need to carefully quantify the rate and extent of each phase of fatigue. Therefore, the purpose of this study was to establish a curve-fitting methodology to provide the best quantitative description of fatigue profiles in isolated mammalian skeletal muscle.

Slow-twitch soleus or fast-twitch *extensor digitorum longus* (EDL) muscles were dissected from mice and bathed in control Krebs solution (4 mM K^+, 147 mM Na^+, 1.3 mM Ca^{2+}, 128 mM Cl^-) at 25°C. With altered K^+ solutions NaCl was exchanged with KCl. Isometric contractions were evoked by supramaximal electric field stimulation (parallel plate electrodes, 20V, 0.1ms pulses). Fatigue protocols involved repeated tetanic stimulation (30-125 Hz) for 500 ms, once every 1-3 s, for 100-300 s. The NLIN procedure available in the SAS statistical software package was used to fit the peak force data from either individual fatigue runs or pooled data from all fatigue experiments.

When fatigue was induced in soleus at 50 Hz for 500 ms, once every second, for 300 s, four distinct phases were apparent. The resulting fatigue profile was extremely well-fitted by a double sigmoid (negative) model with a mean square error of < 1%. The fitting efficacy for a double sigmoid function was better than for single sigmoid, or single and double exponential functions as revealed by the Akaiki Information Criterion. The second sigmoid (*i.e.*, late fatigue) depended on stimulation frequency between 30-125 Hz, and was abolished at the lower frequency of 30 Hz, over 100s. Fatigue induced at 125Hz for 500ms, once every second for 100 s, was well quantified by a double sigmoid model in both soleus and EDL. The first sigmoid (*i.e.*, early fatigue) involved ~10% reduction of peak force to an intermediate plateau in both muscle-types. With the second sigmoid, the maximum rate (slope) was 7-fold greater in EDL than soleus, and the extent of force loss was 83% initial in EDL and 63% initial in soleus. The double sigmoid model was also adequate to describe fatigue induced via nerve terminals, with longer inter-tetanus intervals, or with prolonged continuous tetanic stimulation. We have previously shown that the extent of fatigue is influenced by prior exposure to a physiological range of $[K^+]_o$, in soleus (Cairns, 2005), but there is now a contradictory finding (Zhang *et al.*, 2006). We subsequently utilised the double sigmoid methodology to further analyse our original fatigue data. Fitting parameters for the second sigmoid revealed that the maximum slope, time-constant (τ), and final plateau deteriorated with increasing $[K^+]_o$. For example, τ was 58.0 ± 4.3 s at 2 mM K^+, 52.8 ± 3.4 s at 4 mM K^+, and 43.6 ± 2.4 s at 7 mM K^+. This strengthens our claim that late fatigue is graded with the conditioning $[K^+]_o$.

In conclusion, a double sigmoid expression is a simple method to provide an accurate description of both the rate and extent of different phases of force loss in these models of fatigue.

Burke RE, Levine DN, Tsairis P & Zajac FE. (1973) *Journal of Physiology*, **234:** 723-48.
Cairns SP. (2005) *Proceedings of the Australian Physiological Society*, **36:** 32P.
Lännergren J & Westerblad H. (1991) *Journal of Physiology*, **434:** 307-322.
Zhang S-J, Bruton JD, Katz A & Westerblad H. (2006) *Journal of Physiology*, **572:** 551-9.

This work was supported by a grant from the New Zealand Lottery Grants Board.

Isoform dependent properties of calsequestrin

L. Wei, N.A. Beard and A.F. Dulhunty, John Curtin School of Medical Research, Australian National University, Canberra, ACT 0200, Australia.

Skeletal and cardiac muscle contraction is dependent on Ca^{2+} release from the sarcoplasmic reticulum (SR) through the ryanodine receptor (RyR) calcium release channels. Calsequestrin (CSQ) is the major Ca^{2+} binding protein found within the SR in both skeletal and cardiac muscle, and binds Ca^{2+} with a high capacity and moderate affinity. We have shown that CSQ is a luminal Ca^{2+} sensor for skeletal RyRs (RyR1). However, CSQ1 (skeletal) and CSQ2 (cardiac) are products of different genes and share only 66-80% homology in their primary sequence and are thus likely to differ substantially in their properties and regulation of RyRs. Therefore, we have compared the Ca^{2+} binding capacity of the two isoforms and their ability to associate with and regulate their respective RyRs.

New Zealand male white rabbits were euthanized by a captive bolt and back and leg muscle used to prepare skeletal SR vesicles and CSQ1. Cardiac SR vesicles and CSQ2 were isolated from Merino sheep euthanized by overdose of 20 ml valabarb euthanasia solution (300 mg/ml) injected into the jugular vein. Ca^{2+} binding capacities of rabbit skeletal muscle CSQ1 and sheep cardiac CSQ2 were determined using a ^{45}Ca binding assay and confirmed using Stains-all staining after SDS-PAGE. The fraction of CSQ associated with the SR membrane was quantified following SDS-PAGE of SR fractions and Western blot with antibodies against CSQ1 and CSQ2. RyR channel activity was measured in lipid bilayers. Skeletal or cardiac SR vesicles were reconstituted into artificial planar lipid bilayers which separate two chambers, cytoplasmic and luminal.

We show that there are profound differences between the two isoforms in their Ca^{2+} binding capacity, their association with the RyR and their regulation of RyR activity. Despite the fact that CSQ2 has an extended acidic C-terminal tail (~30 residues longer than CSQ1), CSQ2 binds only half as much Ca^{2+} as CSQ1. To measure the fraction of CSQ associated with RyR, SR fractions (prior to 0.5% Triton X-100 solubilization - using 1 mM Ca^{2+} to retain CSQ's polymer structure), was examined as well as the supernatant and membrane fraction after centrifugation of the solubilized material. We found that 80% of CSQ1, but only 20% of CSQ2, was membrane associated. The ratio of CSQ to RyR in the SR was assessed from solubilized membrane samples using Western blot with anti-CSQ1 and anti-CSQ2 antibodies. The membrane samples contained equal amounts of RyR1 and RyR2 and the anti-CSQ antibodies were used in concentrations which had previously been determined to stain CSQ1 and CSQ2 with equal density. The CSQ/RyR ratio was ~4-fold greater in skeletal SR than in cardiac SR. These results indicate that either CSQ2 is less polymerized at 1 mM Ca^{2+} than CSQ1, or that less CSQ polymer is associated with the triadin/junctin/RyR complex in the cardiac SR.

Native RyR1 or RyR2 in lipid bilayers were treated with Ca^{2+} free luminal solution to depolymerize CSQ and to dissociate all but the residual monomer of CSQ that remains bound to the triadin/junctin/RyR. The effects of adding CSQ back to RyRs was then examined after luminal Ca^{2+} was restored to 1 mM. We found CSQ2 added to native RyR2 activates the channel, in marked contrast to the inhibition of RyR1 by CSQ1 under identical conditions . The inhibitory effect of CSQ1 and RyR1 is highly isoform specific since, at 1 mM luminal Ca^{2+}, CSQ2 activates native RyR1 and CSQ1 activates native RyR2. We have shown previously that CSQ1 regulates native RyR1, which ensures that Ca^{2+} release is decreased during transient reductions in luminal Ca^{2+} concentrations. We are currently investigating the role of CSQ2 in determining the response of native RyR2 to changes in luminal Ca^{2+}. The dissimilar properties of CSQ1 and CSQ2 suggest a differential regulation of their respective SR Ca^{2+} stores which may underlie the strong store depletion with each cardiac contraction, but retention of store Ca^{2+} load in skeletal muscle.

Beard NA, Casarotto MG, Wei L, Varsanyi M, Laver DR & Dulhunty AF. (2005) *Biophysical Journal*, **88:** 3444-54.

Beard NA, Sakowska MM, Dulhunty AF & Laver DR. (2002) *Biophysical Journal* **82:** 310-20.

Wei L, Varsanyi M, Dulhunty AF & Beard NA. (2006) *Biophysical Journal* **91:** 1288-301.

Contractile and fatigue properties of aged fast-twitch EDL muscle from an α-actinin-3 knockout mouse

S. Chan,[1] S.I. Head,[1] J.T. Seto[2] and K.N. North,[2] [1]Department of Physiology, University of New South Wales, NSW 2052, Australia and [2]Faculty of Medicine, University of Sydney, Neurogenetics Research Unit , The Children's Hospital at Westmead, Westmead, NSW 2145, Australia.

The actin-binding protein α-actinin-3 is specifically expressed in fast glycolytic (Type 2B) muscle fibres. Homozygosity for a common polymorphism in the ACTN3 gene results in complete deficiency of α-actinin-3 in about 16% of individuals worldwide. Although α-actinin-3 deficiency does not cause disease in α-actinin-3 knockout mice, recent studies suggest that in young mice (8-10 wks) there is an alteration in the metabolic profile of the fast muscle such that fast-twitch, glycolytic fibres have slower-twitch, more oxidative properties, without an alteration in the overall expression of myosin 2B. To determine the effect of α-actinin-3 deficiency on the physiological properties of skeletal muscle from "aged" animals we studied isolated *extensor digitorum longus* muscles (EDL) from "aged" animals 26 to 31 weeks of age. Animals were sacrificed with an overdose of halothane (ethics approval UNSW). The EDL muscle was dissected from the hindlimb and tied by its tendons to a force transducer at one end and a linear tissue puller at the other. It was placed in a bath continuously superfused with Krebs solution, with composition (mM): 4.75 KCl, 118 NaCl, 1.18 KH_2PO_4, 1.18 $MgSO_4$, 24.8 $NaHCO_3$, 2.5 $CaCl_2$ and 10 glucose, with 0.1% fetal calf serum and continuously bubbled with 95% O_2-5% CO_2 to maintain pH at 7.4. The muscle was stimulated by delivering a supramaximal current between two parallel platinum electrodes. At the start of the experiment, the muscle was set to the optimum length L_0 that produced maximum twitch force. All experiments were conducted at room temperature (~22°C to 24°C).

"Aged" α-actinin-3-deficient muscles showed similar levels of eccentric damage to wild-type muscles following eccentric contractions of 20% strain, 2.6 ± 1.5% in young *c.f.* 1.0 ± 1.7% in "aged" knockouts, suggesting that the absence of α-actinin-3 does not influence the mechanical stability of the sarcomere as the muscle matures. In contrast to younger animals where knockouts showed a slowing of the twitch half-relaxation time, in "aged" knockouts the half-relaxation times were similar (15.4 ± 0.9 ms) to the half-relaxation times (15.8 ± 0.5 ms) recorded in "aged" wild-types. The main effect of aging on the α-actinin-3-deficient muscles was that the significantly better recovery from fatigue reported in young knockouts 30 minutes following a fatigue protocol was even more pronounced, with "aged" knockouts recovering to 85.8 ± 3.0% of their original force, while "aged" wild-types recovered to only 73.4 ± 1.5% of original ($p = 0.004$). These data suggest that the shift in metabolic profile to a slow-twitch profile in α-actinin-3 deficiency becomes even more marked as the animal ages. This may have some beneficial effects on α-actinin-3 deficient "aged" fast-twitch skeletal muscle allowing them to perform repetitive fatiguing tasks at shorter interval than wild-types. Additionally the comparison with "aged" wild-type muscle shows that actinin-3 deficient muscles from young animals appear to be prematurely aged in some of their contractile properties.

Exogenous administration of a PPARδ agonist to dystrophic *mdx* mice confers no protection from contraction-mediated muscle damage

S.M. Gehrig, J.D. Schertzer and G.S. Lynch, Basic and Clinical Myology Laboratory, Department of Physiology, The University of Melbourne, VIC 3010, Australia.

Duchenne muscular dystrophy (DMD) is an X-linked recessive disease caused by a variety of mutations in the dystrophin gene leading to the absence of dystrophin, a cytoskeleton protein implicated in muscle fibre stability. The lack of dystrophin renders muscle fibres highly susceptible to lengthening contraction-induced damage; a contributing mechanism to the dystrophic pathology (Lynch, 2004). Protecting dystrophic muscle fibres from injury is an important therapeutic strategy for DMD. Fast-twitch muscles are more susceptible to contraction-mediated damage than slow-twitch fibres in healthy and dystrophic mice (Consolino & Brooks, 2004), and so altering muscle fibre composition could potentially decrease injury susceptibility. Transgenic over-expression of peroxisome-proliferator activated receptor delta (PPARδ) in skeletal muscles increased the proportion of slow-twitch type I muscle fibres and treating mice with the PPARδ agonist, GW501516, promoted a slow-muscle phenotype and mitochondrial biogenesis, indicative of a shift to higher proportions of type I muscle fibres (Wang *et al*., 2004). We tested the hypothesis that treating dystrophic *mdx* mice with GW501516 would confer protection to muscles from contraction-induced injury by inducing a shift towards a slower muscle phenotype.

Dystrophic *mdx* mice (12 weeks old) were treated with GW501516 (10 mg/kg, oral gavage) for 4 weeks. Mice were anaesthetised deeply (60 mg/kg, sodium pentobarbital) for assessment of contractile function. Susceptibility to contraction-induced injury was examined *in situ* in the tibialis anterior (TA) muscle, and *in vitro* in soleus and diaphragm muscles. Muscle fatigability was examined *in vitro* in the *extensor digitorum longus* (EDL), *soleus*, and diaphragm muscles using a standard four-minute fatiguing stimulation protocol. The mice were killed by cardiac excision while anaesthetised.

Treating *mdx* mice with the PPARδ agonist did not alter the susceptibility to contraction-induced injury in the muscles tested. Maximum force (P_o) was reduced in the TA muscle after treatment. Muscle fatiguability was unchanged in the EDL and diaphragm muscles, however, the soleus muscles were more fatigue resistant after treatment ($p < 0.05$). These results indicate that a minor shift to a slower muscle phenotype does not confer protection to dystrophic muscles from contraction-induced injury.

Consolino CM & Brooks SV. (2004) *Journal of Applied Physiology* , **96:** 633-8.
Lynch GS. (2004) *Clinical and Experimental Pharmacology and Physiology*, **31:** 557-61.
Wang YX, Zhang CL, Yu RT, Cho HK, Nelson MC, Bayuga-Ocampo CR, Ham J, Kang H, & Evans RM. (2004) *PLOS Biology*, **2:** e294.

Supported by the Muscular Dystrophy Association (USA)

Contraction-induced changes to intracellular signalling in skeletal muscle

C. van der Poel, S-A. Tan, S.L. McGee, J.G. Ryall, M. Hargreaves and G.S. Lynch, Department of Physiology, The University of Melbourne, VIC 3010, Australia.

The underlying mechanisms that trigger skeletal muscle adaptations to acute exercise are not well understood. The large mass and intrinsic metabolic capacity of skeletal muscle make it an important tissue in the maintenance of whole-body metabolic homeostasis. Skeletal muscle contraction is associated with increases in $[Ca^{2+}]_i$, energy use and force production. These stimuli are thought to activate intracellular signalling pathways that have downstream effects on gene and protein expression, thus promoting changes to muscle phenotype (Sandström *et al.*, 2007). The aim of this study was to utilize a potent inhibitor of cross-bridge cycling (in fast-twitch muscle), *N*-benzyl-*p*-toluenesulphonamide (BTS), to separate the influences of Ca^{2+}, energy usage, and mechanical force production during muscle contraction, on contraction-sensitive signalling proteins that have downstream effects on gene and protein expression.

Sprague Dawley rats (5-6 weeks of age) were anaesthetised deeply with pentobarbital sodium (60 mg/kg i.p.). *Extensor digitorum longus* (EDL) muscles were carefully excised and either incubated for 1 h in 500 μM BTS or vehicle control (DMSO). Rats were killed by cardiac excision. Following incubation in either BTS or vehicle, muscles underwent a fatigue protocol of 1 tetanic contraction every 5 s for 5 min at a frequency of 80 Hz. Fatigued muscles were either frozen immediately in liquid nitrogen or incubated in Ringer solution for 3 h post-fatigue for later determination of phosphorylated and total levels of calcium/calmodulin-dependent protein kinase isoform II (CaMKII), adenosine monophosphate-activated protein kinase (AMPK) and p38 mitogen-activated protein kinase (MAPK). These kinases are known to play roles in promoting skeletal adaptations to activity.

Phospho-AMPK levels were elevated from basal immediately post-contraction in control groups but not in BTS-treated muscles, indicating that cross-bridge cycling does influence phosphorylation of AMPK. Phospho-CaMKII levels were elevated from basal immediately post-contraction and three hours post-contraction in both groups ($p < 0.05$). The sustained elevations in phospho-CaMKII support previous studies that implicate the Ca^{2+} signal as an initiator of CaMKII activity. Phospho-p38 levels were unchanged from basal immediately post-contraction in both groups. Phospho-p38 was not different from basal in the BTS group at 3 h post-contraction but was increased significantly in the DMSO group.

These findings contribute to our understanding of the underlying mechanisms of exercise-associated metabolic improvements in skeletal muscle, revealing roles for calcium, energy usage, and force production. Specifically, energy and cross-bridge cycling mediate changes in AMPK and p38, and calcium signals mediate changes in CaMKII. Ultimately, the elucidation of pathways involved in improving skeletal muscle metabolism may allow us to identify novel drug targets or design specific exercise programs to assist in maintaining control of whole-body metabolic homeostasis.

Sandström ME, Zhang SJ, Westerblad H & Katz A. (2007) *Journal of Physiology* **579:** 527-34.

This work was supported by grants from the Australian Research Council and the National Health & Medical Research Council.

Quantification of calsequestrin-1 and calsequestrin-2 in rat slow- and fast-twitch skeletal muscle

N.T. Larkins, R.M. Murphy and G.D. Lamb, Department of Zoology, La Trobe University, Melbourne, VIC 3086, Australia.

Calsequestrin is a low-affinity, high-capacity Ca^{2+} binding protein. In muscle, there are two known calsequestrin isoforms, CSQ1 and CSQ2, which are found inside the sarcoplasmic reticulum (SR). CSQ1 is highly expressed in skeletal muscle and can bind a theoretical maximum of ~80 Ca^{2+} per molecule, though probably only ~50 Ca^{2+} per molecule at the maximum free [Ca^{2+}] likely attainable within the SR. CSQ2 is highly expressed in cardiac muscle and can bind up to ~35 Ca^{2+} per molecule at attainable SR [Ca^{2+}]. The relative amounts of CSQ1 and CSQ2 in different fibre types in skeletal muscle are unknown and in the present study we have assessed the relative and absolute amounts of CSQ1 and CSQ2 in rat skeletal muscle. Male Long-Evans hooded rats (6-8 months old) were sacrificed using a lethal overdose of fluothane in accordance with the La Trobe University Ethics Committee and the *extensor digitalis longus* (EDL) and *soleus* (SOL) muscles were excised. For comparisons of EDL and SOL muscles, portions of muscles were homogenized and equal amounts of muscle were analysed by Western blotting using antibodies specific for either CSQ1 or CSQ2. The amount of CSQ1 was greater in EDL muscle homogenates, with SOL muscle homogenates having only about one-third as much CSQ1. There was very little CSQ2 in EDL muscle homogenates and this equated to ~2 % of the CSQ2 found in SOL muscle homogenates. Since SOL muscle is made up of both type I (~85%) and type IIa (~15%) fibres, we further examined the amounts of CSQ1 and CSQ2 in segments of individual fibres dissected from either EDL or SOL muscles. CSQ1 was expressed in all EDL fibres examined and on average SOL fibres expressed ~20% of this amount of CSQ1. CSQ2 was very rarely found in EDL fibres (1 fibre out of 48 fibres examined expressed a similar amount of CSQ2 as in SOL fibres), with there typically being no CSQ2 in EDL fibres and CSQ2 being seen in most SOL fibres. When a SOL fibre did not express CSQ2, it was likely that it was a type IIa fibre. To investigate this further, a number of SOL fibres were mechanically-skinned and individually mounted onto a force transducer and the force responses recorded in Sr^{2+}-based activation solutions at pSr^{2+}(= $-\log_{10}[Sr^{2+}]$) 5.3 and pSr^{2+} 4 (maximum force). It is known that type I fibres exhibit close to maximal force at pSr^{2+} 5.3, whereas type IIa fibres show little or no response at pSr^{2+} 5.3. Out of the 7 SOL fibres examined, 2 fibres showed no force response in pSr^{2+} 5.3, and hence were type IIa fibres. When the same fibres were examined by Western blotting, they were found to express only CSQ1, whereas the other 5 type I SOL fibres all expressed both CSQ1 and CSQ2. To determine the absolute amounts of CSQ1 and CSQ2 in fibres, known amounts of pure CSQ1 and CSQ2 were run on Western blots alongside individual fibres. The amount of CSQ1 was found to be ~100 μM in EDL fibres (n = 6) and ~30 μM in SOL fibres (n = 19) (Note: mM denotes mmol per litre total fibre volume). The amount of CSQ2 in SOL type I fibres was determined to be ~8 μM (n = 9). These concentrations of CSQ1 and CSQ2 fit well with the total SR Ca^{2+} capacities of fibres found previously, which were ~3.6 mM in EDL fibres, ~1.3 mM in SOL type I fibres and likely intermediate in SOL type IIa fibres. It also suggests that at the normal endogenous levels of SR Ca^{2+} (which is ~1.0 to 1.1 mM in all fibre types), in EDL fibres CSQ1 is loaded at only ~20% of the maximal attainable capacity, whereas in SOL type I fibres the CSQ1 and CSQ2 are likely to be loaded at closer to their maximal attainable capacities.

Fryer MW & Stephenson DG. (1996) *Journal of Physiology*, **493:** 357-70.
Trinh HH & Lamb GD. (2006) *Clinical and Experimental Pharmacology and Physiology*, **33:** 591-600.

Protease-activated receptor mediated calcium signaling and cytokine production in cultured c2c12 skeletal muscle cells

A.J. Bakker, K.A. Burlinson, N. Asokananthan, G.A. Stewart and G.J. Pinniger, School of Biomedical, Biomolecular & Chemical Sciences, University of Western Australia, Crawley, WA 6009, Australia.

Protease-activated receptors (PARs) are activated by proteases such as thrombin and tryptase, *via* proteolytic cleavage. In many cells, PAR activation results in a rise in intracellular Ca^{2+} through activation of G_q and phospholipase C, and store-mediated Ca^{2+} entry. This Ca^{2+} signal is thought to trigger the appropriate cellular response. PARs are thought to play a significant role in the inflammatory process, by triggering the release of cytokines from activated cells (Asokananthan *et al.*, 2002). Skeletal muscle myotubes express PAR receptors, and increased intracellular Ca^{2+} has recently been shown to increase the production of inflammatory cytokines such as IL-6 in muscle cells (Keller *et al.*, 2006). In this study, we examined the nature of PAR-mediated Ca^{2+} signaling in cultured skeletal muscle myotubes and determined whether PAR activation resulted in the release of the cytokine IL-6 from these cells.

C_2C_{12} myoblasts were grown in Dulbecco's modified Eagles medium with 20% foetal calf serum and equilibrated with 5% CO_2, 95% air at 37°C. Differentiation of myoblasts into myotubes was induced by lowering the serum concentration to 2%. PARs were activated with thrombin (activates PAR-1, 3 & 4 isoforms) and trysin (activates PAR-2 isoform. The intracellular Ca^{2+} concentration was measured using the fluorescent Ca^{2+} indicator fura-2. Measurements were undertaken using a Cairn Spectrophotometer. Experiments were undertaken at 22°C and IL-6 levels were detected by ELISA.

Exposure of the myotubes to thrombin resulted in a significant increase in intracellular Ca^{2+} (mean amplitude; 0.38 ± 0.03 μM, $n = 13$) that was larger in peak than electrically-induced Ca^{2+} transients elicited in similar C_2C_{12} myotubes (mean amplitude; 0.20 ± 0.07 μM, $n = 11$). Pre-exposure to thrombin (10 U/ml) for one hour, 12 hours before experimentation resulted in 93% of myotubes responding to thrombin with a Ca^{2+} response. Experiments with specific PAR-activating peptides indicated that thrombin was activating Ca^{2+} signalling *via* PAR-1. In myotubes exposed to thrombin under Ca^{2+} free conditions, only 17% ($n = 6$) of myotubes displayed Ca^{2+} influx upon return of extracellular Ca^{2+}. In addition, only 12% of cells ($n = 17$) responded with Ca^{2+} influx after the store was depleted with the sarcoplasmic reticulum Ca^{2+} pump inhibitor 2,5-di-(tert-butyl)-1,4-benzohydroquinone, suggesting that in most myotubes, store-operated Ca^{2+} entry was absent. Exposure of myotubes to thrombin (5 U/ml) for 24 hours increased IL-6 levels to 140% of control levels ($p = 0.01$). Pre-exposure to thrombin (10 U/ml) for one hour, followed by a 24 hour exposure to thrombin (5 U/ml) 12 hours later, increased IL-6 levels to 188% of control levels ($p = 0.01$).

These results suggest that the Ca^{2+} signal associated withevoked by PAR-1 activation is predominantly associated with intracellular Ca^{2+} release, and that thrombin exposure results in the release of the IL-6, which may play a role in the muscle response to injury and inflammation.

Asokananthan N., Graham PT, Fink J, Knight DA, Bakker AJ, McWilliam AS, Thompson PJ & Stewart GA. (2002) *Journal of Immunology*, **168:** 3577-85.

Keller C., Hellsten Y., Steensberg A. & Pedersen BK. (2006) *Cytokine*, **36:** 141-7.

TRPC3 and GLUT4 interact during insulin-mediated glucose uptake in adult skeletal muscle

H. Westerblad, J.T. Lanner, D. Severa, S.L. Zhang, Y. Assefaw-Redda and J.D. Bruton, Department of Physiology and Pharmacology, Karolinska Institutet, 171 77 Stockholm, Sweden.

We examined the role of the Ca^{2+} permeable canonical transient receptor potential 3 (TRPC3) channels in insulin-mediated glucose uptake in skeletal muscle. Adult male mice were killed by rapid neck disarticulation and the hindlimb flexor digitorum brevis (FDB) muscles were removed. The study was approved by the Stockholm North local ethical committee. Intact, single muscle cells were isolated from the FDB muscles and TRPC3 was knocked down with siRNA, which was introduced into the cells with a novel transfection technique involving carbon nanotubes. TRPC3 expression in siRNA treated cells was decreased by ~40% and this was accompanied by ~80% decrease in insulin-meidated glucose uptake. TRPC3 can be directly activated by diacylglycerol (DAG) and knock down of TRPC3 inhibited DAG-induced Ca^{2+} influx. TRPC3 was detected in GLUT4 immunoprecipitates. Immunofluorescence staining showed a clear overlap between TRPC3 and GLUT4 in the proximity of the t-tubular system, which is the major site of insulin-mediated glucose uptake in skeletal muscle. In conclusion, TRPC3 functionally and physically interacts with GLUT4 in skeletal muscle and Ca^{2+} influx through TRPC3 has a large impact on the insulin-mediated glucose uptake.

Whole-body cooling during hyperthermia: physiology versus physics

J.N. Caldwell,[1] A.M.J. van den Heuvel,[1] M.J. Patterson[2] and N.A.S. Taylor,[1] [1]School of Health Sciences University of Wollongong Wollongong NSW 2522 Australia and [2]Defence Science and Technology Organisation Melbourne VIC Australia.

Heat exhaustion and illness frequently occur without warning, and are often characterised by a rapid onset. In clinically-significant cases, patient cooling time can impact upon the prognosis. For inanimate objects, the rate of heat loss is a simple function of the thermal gradient that can be established, thus, immersion in ice-cold water is an effective means to rapidly extract heat. However, access to ice or cold water is limited in hot climates in the field, and there are also clinical concerns regarding sudden cold-water immersion in hyperthermic individuals. Furthermore, sympathetically-mediated cutaneous vasoconstriction reduces convective heat transfer from the core. It was therefore hypothesised that a warmer immersion, in which vasoconstriction is less powerful, may facilitate rapid cooling in hyperthermic individuals. To test this hypothesis, eight males participated in three trials, consisting of separate heating and cooling phases. Subjects were heated over 95 min to an oesophageal temperature of 39.5°C, using exercise in the heat (36°C, 50% relative humidity and water-perfusion garment (40°C)). Heating followed a fixed protocol to achieve three target oesophageal temperatures (38.5°C, 39.0°C, 39.5°C), sustained for 30, 20 and 10 min (respectively). Following a 5-min preparation, subjects were cooled using one of three methods: air (20-22°C: control); cold-water immersion (14°C); temperate immersion (26°C). After heating, oesophageal temperatures were 39.4°C (control), 39.3°C (cold immersion) and 39.3°C (temperate immersion). The time taken to reach the target core temperature (37.5°C; Figure) averaged 24.78 min (control), 2.84 min (cold immersion) and 4.56 min (temperate immersion), with each of the between-trial comparisons being statistically significant ($P < 0.05$).

Cooling in water, which has a thermal conductivity > 24 times that of air, will always be more rapid. Nevertheless, it is clear that whole-body cooling in temperate water takes only marginally longer than cold-water cooling. Indeed, one cannot imagine that the time difference of 1.72 min could have any meaningful physiological or clinical implications. In cold water, cutaneous vasoconstriction is maximised, with transcutaneous heat loss being dependent upon conduction. In temperate water, it was assumed that the rapid heat loss was due to a less powerful vasoconstrictor response, with central heat being rapidly transported (convective flow) to the skin surface for dissipation. While the core-to-water thermal gradient was much less during this immersion, a presumably higher skin blood flow supported the rapid convective delivery of heat to the skin, and its subsequent dissipation. Thus, a sustained physiological mechanism (skin blood flow) has countered a less powerful thermal gradient, resulting in clinically insignificant differences in heat extraction.

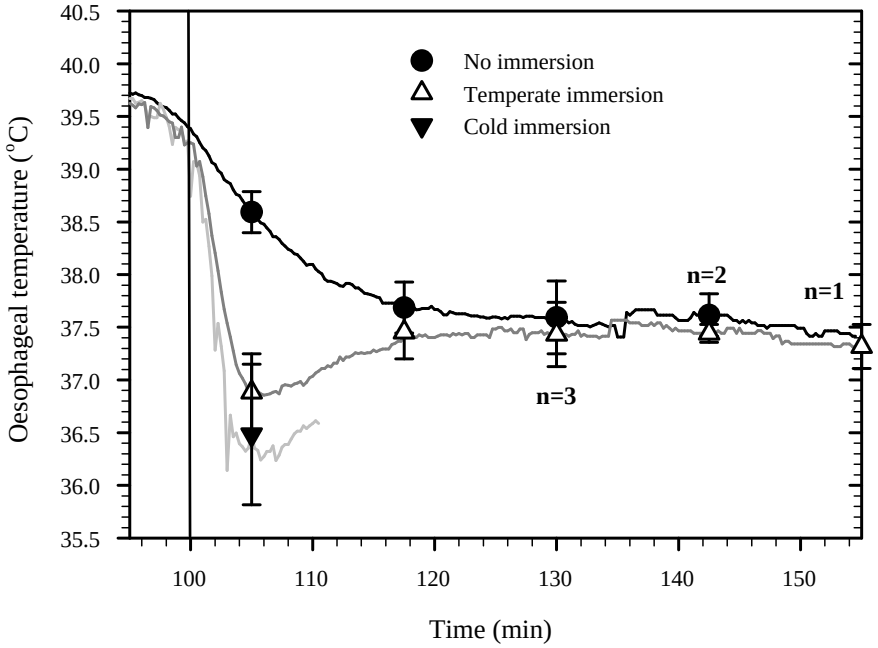

Resistance training increases total AKT, but decreases basal AS160 phosphorylation in individuals with clusters of metabolic risk factors

C.A. Goodman,[1] I. Levinger,[1] K.F. Howlett,[2] J. Peake,[3] A. Garnham,[2] D.L. Hare,[4] G. Jerums[5] and S. Selig,[1]
[1]School of Human Movement, Recreation and Performance, Victoria University, Melbourne, VIC 8001, Australia, [2]School of Exercise and Nutrition Sciences, Deakin University, Melbourne, VIC 3125, Australia, [3]School of Human Movement Studies, University of Queensland, Brisbane, QLD 4072, Australia, [4]Department of Cardiology, Austin Health, University of Melbourne, VIC 3084, Australia and [5]Department of Endocrinology, Austin Health, University of Melbourne, VIC 3084, Australia.

An increased risk profile and levels of inflammatory markers may lead to abnormal glucose homeostasis, insulin resistance and type 2 diabetes. Studies have reported that obesity and diabetes impairs the phosphatidylinositol 3- kinase (PI3-K) pathway, partly by reducing phosphorylation and activity of the insulin signalling proteins Akt and Akt substrate of 160kDa (AS160) (Krook *et al.*, 2004; Krook *et al.*, 1998; Karlsson *et al.*, 2005). Aerobic training has been shown to improve insulin signalling protein phosphorylation and improve insulin sensitivity. The effect of resistance training (RT) on insulin signalling proteins however is less clear. Howlett *et al*. (2007) recently reported that AS160 phosphorylation decreases immediately after an acute bout of resistance exercise. To date, no studies have examined the effect of prolonged resistance training on basal AS160 phosphorylation. Also, limited data exist concerning the association between inflammatory markers, metabolic risk factors and total and phosphorylated forms of Akt and AS160. Therefore, this study investigated the effects of RT, as a single intervention, on total and phosphorylated forms of Akt and AS160 in individuals with clusters of metabolic risk factors, and the correlation between these proteins, metabolic risk factors and inflammatory markers in this population.

Twenty-one untrained men (n = 13) and women (n = 8) aged 51.2 ± 1.5 (Mean ± SEM; range 40-69 yr), who had two or more risk factors for metabolic syndrome (International Diabetes Federation; Zimmet *et al.,* 2005) were randomly allocated to training (n = 10) or non-exercise control (n = 11) groups. Randomisation was stratified according to sex. RT was performed 3 days a week for 10 weeks with a gradual increase in intensity from 40-50% of one repetition maximum (1RM) to 80-85% of 1RM (see Levinger *et al.,* (2007) for details). Before and after the RT, anthropometric measurements were conducted, resting muscle biopsies (*vastus lateralis*) were obtained, and blood samples were collected for inflammatory markers (IL-1β, IL-6, IL-8, IL-10 & TNF-α). To obtain 'basal' levels of Akt/AS160 phosphorylation and systemic markers of inflammation, the post-training muscle biopsy and blood samples were taken 4-5 days after the last training bout to minimise any acute changes due to the last training stimulus. Muscle samples were analysed for total and phosphorylated forms of Akt and AS160 by Western blotting and for muscle glycogen content. Results are Mean ± SEM.

Pre-training (baseline), the two groups did not differ significantly in terms of sex, age, anthropometric measurements or metabolic risk factors. At baseline, with all participants combined, there were positive correlations between total Akt and total AS160 (r = 0.48, p = 0.03) and the phosphorylated forms of Akt (Ser^{473}) and AS160 (r = 0.65, $p < 0.01$). RT significantly increased total Akt from 172.8 ± 15.9 to 215.8 ± 27.1 arbitrary units (or 22.5 ± 8.2 % increase; $p < 0.01$ compared to pre-training value and p = 0.06 compared to controls) and reduced basal AS160 phosphorylation from 95.1 ± 18.2 to 71.5 ± 13.9 arbitrary units (or 19.9 ± 12.3 % decrease; p = 0.02 compared to pre-training data and p = 0.01 compared to controls). RT did not significantly alter basal Akt (Ser^{473}) phosphorylation or total AS160 protein content. Also, these proteins did not change in the Control group. RT did not alter the plasma levels of inflammatory markers. RT tended to increase glycogen stores (27.4 ± 10.9%, p = 0.06). The percentage change in phosphorylated AS160 was negatively correlated with the number of metabolic risk factors (r = 0.81, $p < 0.01$) and with plasma HbA1c (r = 0.74, p = 0.02).

In summary, 10 wks of RT increased total Akt protein content and reduced the basal levels of AS160 phosphorylation in middle aged people with high increased numbers of metabolic risk factors. The implications of this result for insulin signaling and glucose homeostasis remain to be determined.

Howlett KF, Sakamoto K, Garnham A, Cameron-Smith D & Hargreaves M. (2007) *Diabetes*, **56:** 1608-14.
Karlsson HK, Zierath JR, Kane S, Krook A, Lienhard GE & Wallberg-Henriksson H. (2005) *Diabetes*, **54:** 1692-97.
Krook A, Roth RA, Jiang XJ, Zierath JR & Wallberg-Henriksson H. (1998) *Diabetes*, **47:** 1281-6.
Krook A, Wallberg-Henriksson H & Zierath JR. (2004) *Medicine and Science in Sports and Exercise*, **36:** 1212-17.
Levinger I, Goodman C, Hare DL, Jerums G & Selig S. (2007) *Diabetes Care*, **30:** 2205-10.
Zimmet PZ, Alberti KG & Shaw JE. (2005) *Medical Journal of Australia*, **183:**175-176.

Inhibitors of mitochondrial function disrupt uterine pacemaking

F.S. Gravina,[1] K. Ryan,[1] M.S. Imtiaz,[1] S.L. Sandow,[2] R. Smith,[3] H.C. Parkington[4] and D.F. van Helden,[1] [1]School of Biomedical Sciences, Faculty of Health, University of Newcastle, NSW 2308, Australia, [2]Department of Pharmacology, University of New South Wales, NSW 2052, Australia, [3]Mothers and Babies Research Centre, John Hunter Hospital & School of Medicine and Public health, University of Newcastle, NSW 2308, Australia and [4]Department of Physiology, Monash University, VIC 3800, Australia.

Natural birth occurs through rhythmic contractions of the smooth muscle of the uterus. However, there is surprisingly little understanding of the mechanism of the pacemaker clock that both initiates and times the remarkable regularity of uterine contractions of labour. We aim to investigate whether store pacemaking, a mechanism where the release-refill cycle of entrained intracellular stores acts as the pacemaker clock, has a role in uterine pacemaking. This mechanism was first shown in lymphatic smooth muscle and functions through entrainment of stores through coupled oscillator-based interactions, with sub-plasmalemmal Ca^{2+} release interacting with channels in the cell membrane to activate a pacemaker current (see van Helden & Imtiaz, 2003). However, uterine pacemaking may be different, in that agents that inhibit the SERCA pump and hence presumably block store function do not inhibit spontaneous uterine contractions. The present study is a first stage investigation of mechanisms that may contribute to pacemaking, focusing on the role of mitochondria.

Experiments were on single bundle strips (diameter = 100-300 μm; length = 2-4 mm) of longitudinal smooth muscle dissected from the uterus of freshly killed young adult mice (age 5-8 weeks). Mice were euthanased by overexposure to the inhalation anaesthetic isoflurane (5-10% in air), a procedure approved by the Animal Care and Ethics Committee at the University of Newcastle. The strips were secured in a 1-3 ml chamber and superfused at 1-5 ml/min with oxygenated (95% O_2, 5% CO_2) physiological saline of composition (mM): NaCl (120), KCl (5), $CaCl_2$ (2.5), $MgCl_2$ (2), $NaHCO_3$ (25), NaH_2PO_4 (1), glucose (10), with a pH of 7.3 at 35ºC. In most cases pacemaking was measured using video recording of spontaneous contractions. Some recordings were also made using intracellular microelectrodes (resistance 100-150 MΩ filled with 1 M KCl), though for this tissues generally needed to be immobilised by Wortmannin, an agent that blocks myosin light chain kinase and inhibits uterine contractions without marked effects on pacemaker function. A third procedure was to monitor pacemaking through Ca^{2+} imaging using a high speed Nipkow spinning disk system. In this case strips were pre-loaded with 5-10 μM Oregon Green/AM for 1 h at room temperature. Strips were either spontaneously active or could be induced to exhibit pacemaker activity by application of oxytocin (3 nM). In the case of the latter, oxytocin was applied throughout (*i.e.*, before and during the test procedures). Two classes of agents that inhibit aspects of mitochondrial function have been tested so far. The first was the mitochondrial uncoupler CCCP (1 μM), which is a protonophore that decreases the transmembrane potential across the inner mitochondrial membrane. The second class of inhibitor was the respiratory chain (complex I) inhibitor rotenone (3 μM). Both agents initially enhanced and then markedly decreased or abolished uterine pacemaking. These effects were unlikely to be due to depletion of ATP as pacemaking persisted in the presence of oligomycin (5 μM), an agent known to block the F1/F0 ATP synthase. These data are enticing as they indicate that mitochondria have a seminal role in store pacemaking. How this is achieved needs to be determined. The data do not exclude a role for store pacemaking, as it has been demonstrated in intestinal wall that inhibition of mitochondrial function disrupts store pacemaking (Ward *et al.*, 2000).

van Helden DF & Imtiaz MS. (2003) *Journal of Physiology*, **548:** 271-96.

Ward SM, Ordog T, Koh SD, Abu Baker S, Jun JY, Amberg G, Monaghan K & Sanders KM. (2000) *Journal of Physiology*, **525:** 355-61.

Differential inhibitory signalling in the superficial and deep dorsal horn of the mouse spinal cord

W.B. Anderson,[1,2] B.A. Graham,[1,2] P. Jobling,[1,2] P.A. Tooney,[1,2] A.M. Brichta[1,2] and R.J. Callister,[1,2] [1]School of Biomedical Sciences, University of Newcastle, Callaghan, NSW 2308, Australia and [2]Hunter Medical Research Institute (HMRI), Lookout Road, New Lambton, NSW 2310, Australia.

Neurons in the superficial (SDH; laminae I-II) and deep (DDH; laminae IV-VI) dorsal horn of the spinal cord receive synaptic inputs from the periphery via small and medium diameter afferent fibres, respectively. Both regions have well-established, although largely separate, roles in the spinal processing of pain signals. Despite this, fast synaptic inhibition is provided by glycine- and $GABA_A$- receptors in both regions under normal conditions and both receptor types been implicated in the onset and maintenance of pathological pain states. Until recently, glycine receptors (GlyRs) throughout the adult nervous system were thought to be composed of α1/β-subunits, however an unusual form of the GlyR, containing α3-subunits, has recently been identified in the SDH, but not the DDH (Harvey *et al.*, 2004). Moreover, tonic inhibitory drive mediated by glycine and $GABA_A$ receptors differs in the superficial and deep layers of the dorsal horn (Cronin *et al.*, 2004). To further understand the contribution of these two inhibitory transmitter systems in spinal pain processing, we compared the electrophysiological properties of synaptically located GlyRs and $GABA_A$Rs in the SDH and DDH. Mice (C57Bl/6, both sexes, P17-37) were anaesthetised (Ketamine, 100 mg/kg, i.p.) and decapitated. Transverse slices (300 um thick) were prepared from the spinal cord (L3-L5 segments) and voltage-clamp recordings were made from SDH and DDH neurons (CsCl internal; holding potential 70 mV; 23ºC). Strychnine-sensitive (1 um) glycinergic mIPSCs were recorded in the presence of tetrodotoxin (1 μM), CNQX (10 μM) and bicuculline (10 μM). Bicuculline-sensitive (10 μM) $GABA_A$ergic mIPSCs were recorded in the presence of tetrodotoxin (1 μM), CNQX (10 μM) and strychnine (1 μM). Glycinergic mIPSCs were detected in 23/35 SDH neurons, but were observed in all DDH neuron recordings (20/20). In contrast, $GABA_A$ergic mIPSCs were present on all (n = 15) neurons tested in the SDH, but on only 15/18 neurons in the DDH. Several properties of the two receptors also differed in the SDH and DDH. For example, glycinergic mIPSC amplitude was smaller (38.0 ± 3.2 *vs.* 55.5 ± 5.6 pA; $p < 0.05$), mIPSC decay time was slower (10.3 ± 0.5 *vs.* 5.1 ± 0.4 ms; $p < 0.05$), and mIPSC frequency was lower (0.24 ± 0.04 *vs.* 0.90 ± 0.17 Hz; $p < 0.05$) in SDH *vs* DDH neurones. In contrast, $GABA_A$ergic mIPSCs had similar amplitudes (15.6 ± 1.3 *vs.* 16.2 ± 2.2 pA) and frequencies (0.16 ± 0.06 *vs.* 0.18 ± 0.06 Hz); however, decay times were also slower (23.0 ± 2.4 *vs.* 12.3 ± 0.8 ms) in SDH *vs* DDH neurones. Interestingly, the mean single channel current underlying these mIPSCs, estimated using peak-scaled non-stationary noise analysis, was identical in both regions for GlyR (3.9 ± 0.7 pA, n = 11 *vs.* 3.8 ± 0.7, n = 8) and $GABA_A$R (1.6 ± 0.1 pA, n = 10 *vs.* 1.6 ± 0.2 pA, n = 11). These electrophysiological data were compared with results from real-time PCR analysis of the expression of GlyR subunits (α1-4 and β) in the SDH and DDH. The α1 subunit gene was highly expressed in both SDH and DDH, although levels were increased three-fold in the SDH. The β subunit was also highly expressed throughout the dorsal horn, however levels were three-fold higher in the DDH. The expression of α3 subunit was lower, relative to α1 and β subunits, but at three fold higher levels in the SDH *vs.* DDH. Together, these data indicate that glycine and $GABA_A$ receptors with differing physiological properties contribute to fast synaptic inhibition in deep and superficial regions of the mouse dorsal horn. These features are likely to influence pain processing differently in the SDH and DDH and provide a basis for selectively modifying inhibition in the two regions.

Cronin JN, Bradbury EJ, & Lidierth M. (2004) *Pain*, **112:** 156-63.
Harvey RJ, Depner UB, Wassle H *et al.* (2004) *Science*, **304:** 884-7.

Maturation of neuron excitability and membrane conductances in the superficial dorsal horn of the mouse spinal cord

M.A. Walsh,[1,2] B.A. Graham,[1,2] A.M. Brichta[1,2] and R.J. Callister,[1,2] [1]School of Biomedical Sciences, University of Newcastle, Callaghan, NSW 2308, Australia and [2]Hunter Medical Research Institute (HMRI), New Lambton, NSW 2305, Australia.

Neurons in the superficial dorsal horn (SDH; laminae I-II) of the spinal cord play a critical role in processing nociceptive, thermal and tactile information. As in other CNS regions the output of SDH neurons is determined by the combined action of synaptic inputs, and intrinsic membrane properties. It is well established that synaptic inputs in the SDH, especially those of primary afferents, undergo extensive reorganization during early postnatal development. It is unclear, however, whether or how interneuron excitability and membrane conductances change during development. In this study we assessed membrane properties and whole cell currents in SDH interneurons during late embryonic (E15-17) and early postnatal (P0-25) development. Mice (C57Bl/6) were anaesthetised with Ketamine (100 mg/kg, i.p.) and decapitated. Transverse slices were prepared from the lumbar spinal cord (segments L3-L5). Whole-cell patch-clamp recordings were obtained from SDH neurons at 32ºC using a KCH_3SO_4based internal solution. Data were grouped into one embryonic and five postnatal developmental stages (E15-17, n = 51 neurons; P0-5, n = 60; P6-10, n = 49; P11-15, n = 54; P16-20, n = 49; and P21-25, n = 52). Several passive and active membrane properties changed dramatically over this period. For example, input resistance decreased from over 1000 MΩ; at E15-17 to ~ 400 MΩ; in P21-25 neurons, and resting membrane potential became more hyperpolarized (-53.8 ± 1.5 to 63.4 ± 1.4 mV) over the same period. Action potential (AP) properties such as spike amplitude and afterhyperpolarization amplitude increased (24.9 ± 1.8 versus 43.2 ± 1.6 mV; 10.1 ± 1.8 versus 31.0 ± 0.9 mV, respectively), whereas AP half-width decreased (2.7 ± 0.4 versus 1.2 ± 0.1 ms). Comparisons of mean values for the above variables in the six age groups revealed that the transition from embryonic/neonatal to adult-like passive and active membrane properties occurred around P6-10. We next examined the discharge properties of SDH neurons in response to step-current injection (800 ms, 20 pA increments). Neurons were assigned into five categories according to AP discharge patterns: *tonic firers* fired spikes throughout the step duration; *initial bursters* fired several spikes at step onset; *single spikers* fired one or two spikes at step onset; *delayed firers* did not fire spikes until well after step onset; and *reluctant firers* did not fire APs during current steps. Before birth (E15-17) *single spikers* dominated the sample (>50%), and *delayed firers* were not observed. Soon after birth (P0-10) *single spikers* still dominated (~41%) and *delayed firers* were rare (< 1%). In older animals (P11-25) *initial bursters* dominated (~ 40%) and all five firing patterns were well represented. Investigation of the major subthreshold currents that contribute to the above discharge categories showed the rapid A-type potassium current (I_{Ar}) dominated at all ages examined. In embryonic neurons almost all neurons (> 95%) had I_{Ar}. This decreased to ~50% of neurons after P10. Together, these data indicate that the membrane properties and excitability of SDH neurons undergo major alterations during development, with the critical period for these changes occurring around P6-10.

Compensatory changes in rapid A-type potassium channel function in the superficial dorsal horn of the spastic mouse; studied *in vitro* and *in vivo*

B.A. Graham,[1] P.R. Schofield,[2] A.M. Brichta[1] and R.J. Callister ,[1] [1]School of Biomedical Sciences, University of Newcastle, Callaghan, NSW 2308, Australia and Hunter Medical Research Institute (HMRI), New Lambton, NSW 2305, Australia and [2]Prince of Wales Medical Research Institute (POWMRI), Randwick, NSW 2031, Australia.

The spastic mouse has a naturally occurring mutation in the inhibitory glycine receptor. Previously we have shown that the spastic mutation disrupts synaptic transmission in both motor (Graham *et al.*, 2006) and sensory (Graham *et al.*, 2003) pathways by reducing glycinergic inhibition. In addition to disrupted glycinergic inhibition, we have also identified a concomitant increase in $GABA_A$ergic inhibition in the superficial dorsal horn (SDH) of the spastic mouse (Graham *et al.*, 2003). The impact of this altered inhibitory drive on signal processing and neuronal excitability in the SDH of the spastic mouse has not been investigated. In this study, we used a combination of *in vitro* and *in vivo* patch-clamp recording techniques to examine how altered inhibitory drive affects neuron excitability and signal processing in the SDH of the spastic mouse. For *in vitro* experiments, mice (C57Bl/6 or spastic; ~ P23) were anaesthetised with Ketamine (100 mg/kg, i.p.) and decapitated. Transverse slices (300 μm thick) were prepared from the lumbar spinal cord (L3-L5 segments). Intrinsic membrane properties and excitability of spastic and wildtype SDH neurons (n = 91 and 97 neurons, respectively) were compared using whole-cell current and voltage-clamp recording techniques (KCH_3SO_4 internal solution; 23°C). Apart from a modest reduction (-69.2 ± 0.8 *vs.* -66.6 ± 0.8 mV; $p < 0.05$) in resting membrane potential, neurons in the spastic mouse had membrane and action potential (AP) properties identical to those of wildtype mice. There was, however, a substantial reorganization of AP discharge patterns in response to step current injection (800 ms, 20 pA increments). Recordings in spastic, showed a significant increase (14%) in the proportion of delayed firing neurons, compared to wildtype controls. We also observed a depolarising shift in the steady-state inactivation of rapid A-currents (I_{Ar}), an important potassium conductance in SDH neurons. We propose that this shift in voltage sensitivity of I_{Ar} enhances its impact on delaying AP discharge and increases the proportion of delayed firing neurons in the SDH. To assess the functional consequences of the reorganization of AP discharge patterns and enhanced I_{Ar} current on signal processing in the SDH we next made *in vivo* patch-clamp recordings from spastic and wildtype SDH neurons (n = 32 and 37, respectively). Mice (~ P37) were deeply anaesthetised (Urethane 2.2 g/kg, i.p.) and SDH neuron responses to innocuous (brush) and noxious (pinch) hindpaw stimulation were quantified. Overall, responses recorded in wildtype and spastic mice were similar (p = 0.21); however, in spastic mice a small population of spontaneously active neurons (~ 10 %) exhibited elevated spontaneous discharge frequency and post-pinch discharge rates. Together, these results are consistent with the altered intrinsic membrane properties of SDH neurons, observed *in vitro*, having functional consequences for pain processing mechanisms *in vivo*. We propose that alterations in I_{Ar} current properties in the spastic mouse compensate, in part, for disrupted inhibition and maintain normal signal processing in the SDH.

Graham BA, Schofield PR, Sah P, & Callister RJ. (2003) *Journal of Physiology*, **551:** 905-16.
Graham BA, Schofield PR, Sah P, Margrie TW, & Callister RJ. (2006) *Journal of Neuroscience,* **26:** 4880-90.

Voltage dependent currents in type I and II hair cells and calyx terminals of primary afferents in an intact vestibular preparation

A.E. Kindig, R. Lim, R.J. Callister and A.M. Brichta, Hunter Medical Research Institute, School of Biomedical Sciences, Faculty of Health, University of Newcastle, Callaghan, NSW 2308, Australia.

Mammalian vestibular end-organs contain type I and type II hair cells that are responsible for the conversion of mechanical stimuli into neural signals. These signals are then transmitted through chemical synapses to primary afferent fibers and passed on to the central nervous system. Precisely how hair cells and primary afferents communicate is unknown. Most studies to date have concentrated on isolated hair cells with little regard to their effects on primary afferents. Here we describe our initial recordings from an intact epithelial preparation that will help us understand how these two important components of our peripheral balance system interact.

From previous studies we know that the two types of hair cells not only differ morphologically but also functionally. For example, the type I hair cells are amphora-shaped and most of the basolateral surface of the type I cell is ensheathed in the dendritic cup-like or "calyx" ending of the primary afferent. In contrast, barrel-shaped type II hair cells are contacted by simple synaptic boutons. The precise function of the calyx ending and the influence it exerts upon synaptic transmission between the type I hair cell and its primary afferent remains a mystery. Our major effort, therefore, is to understand this unique synapse. Functionally, type I hair cells exhibit a large outward current (termed $I_{K,L}$) at resting membrane potential, whereas type II hair cells do not. $I_{K,L}$, therefore, confers a very low impedance (about 10Ω) to type I hair cells at rest. Theoretically, this low impedance makes it difficult, if not impossible, for these hair cells to depolarize enough for normal neurotransmitter release by even the largest currents induced by movement of their apical hair bundles. The unusual architecture of the calyx ending, however, may provide a clue. Since the calyx forms a long narrow synaptic cleft, it may allow for significant potassium (K^+) accumulation thereby contributing to significant depolarization of its hair cell and primary afferent terminal. This, in turn, would not only allow neurotransmitter release but would also make the primary afferent itself more excitable. To date, previous studies have been unable to test this hypothesis because most experiments have used whole cell "dissociated" preparations, where the calyx terminal has been removed. Our intact *in vitro* preparation, taken from deeply anesthetized mice (ketamine 100 mg/kg, i.p.) is a novel approach in that we preserve the hair cells within the crista. This allows us to record from type I hair cells while they are still contacted by the calyx terminal ending. Using the whole-cell patch-clamp technique we have begun to record from type I hair cells and their associated calyx ending, as well as type II hair cells. This is the first step in developing a viable preparation in which we will clarify how information is passed between the hair cell and the primary afferent.

Funding provided by NHMRC, Garnett Passe and Rodney Williams Memorial Foundation, HMRI and the Meniere's Research Fund.

Vestibular effects of ionic and volume changes of inner ear fluid in an isolated preparation of a mouse labyrinth

E.G. LaMont, R. Lim, R.J. Callister and A.M. Brichta , Hunter Medical Research Institute, School of Biomedical Science, The University of Newcastle, University Drive, Callaghan, NSW 2308, Australia.

We have developed an *in vitro* preparation of the mouse inner ear to examine pharmacological and physiological features of balance (vestibular) transduction that cannot be easily addressed in whole animal or dissociated hair cell preparations. Having established the preparation's response to manipulation of the external (perilymphatic) compartment (Lee *et al.*, 2005), we have now begun investigating the effects of changing the internal (endolymphatic) compartment.

Mice were anaesthetized (ketamine 100 mg/kg, i.p.), decapitated, and the bony labyrinth was surgically isolated from the skull by removing, *in toto,* the petrous portion of the temporal bone. The tissue was placed into a recording chamber and maintained in Ringer's solution. Apertures were created in the bony labyrinth to access the underlying membranous ducts and nerve fibres. A bevelled, glass injecting pipette (10-15 μm tip diameter) was inserted into either the exposed endolymphatic or semicircular canal duct. The pipette was attached to a nanoliter injection pump that allowed us to introduce solutions of precisely controlled ionic concentrations and volumes into the duct. Sharp recording electrodes were used to impale individual primary afferent fibres in the anterior or horizontal ampullary nerves. Primary afferent action potential (AP) discharge was recorded during manipulation of endolymphatic composition and volume.

Our aim was to assess the effects of high potassium (K^+) concentration and increased volume on AP discharge, two factors thought to be associated with Ménière's disease. As might be expected, injections of high K^+ solution (200 mM KCl, 25 mM $KHCO_3$) into the semicircular canal duct caused a 4 to 5 fold increase in discharge rate (n = 5). This was accompanied by diminishing AP amplitude as the afferent became depolarized. Within 15 s to 2 min after injection of high K^+ solutions, AP firing rate and amplitude returned to original levels, suggesting a return to prior conditions. While a majority (6 of 10) injections of 'normal' artificial endolymph (140 mM KCl, 25 mM $KHCO_3$) produced similar results to those seen with high K^+ solution, a few (4 of 10) injections of 'normal' endolymph resulted in decreases in discharge rate. We have begun to explore the potential mechanisms underlying these anomalous results and hypothesise that it is the location of the afferent terminal, within the neuroepithelium, that ultimately determines its response to endolymphatic volume changes.

Taken as a whole, our results suggest that: 1) we can affect afferent activity by altering the ionic composition of the endolymphatic compartment; and 2) volume changes play a significant role in modifying afferent activity.

Lee H-Y, Camp AJ, Callister RJ & Brichta AM. (2005) *Journal of Neuroscience Methods*, **145:** 73-87

Acknowledgements: Garnett Passe and Rodney Williams Memorial Foundation; Australian-American Fulbright Commission; Meniere's Research Fund; National Health and Medical Research Council of Australia.

Inhibitory synaptic transmission in neurons of the medial vestibular nucleus after unilateral labyrinthectomy

R. Lim, R.J. Callister and A.M. Brichta, Hunter Medical Research Institute, School of Biomedical Sciences, The University of Newcastle, University Drive, Callaghan, NSW 2308, Australia.

Introduction. Loss of peripheral balance (vestibular) organs from one side of the head or unilateral labyrinthectomy (UL) causes stereotypical behaviour in all animals and includes head tilt toward the ablated side, circling, barrel-rolling, and spontaneous nystagmus (eye flicking). Within a few days after UL, many of these symptoms abate. This recovery is referred to as "vestibular compensation" and is due entirely to changes in central activity since there is no regeneration of peripheral organs within this period. Precisely how and where this compensation occurs is unknown.

It has been suggested that much of this "compensation" occurs in the vestibular nuclei, the primary target for incoming vestibular afferents. *In vivo* studies have shown in the acute phase of vestibular compensation, ipsilesional neurons in the medial vestibular nucleus (MVN) are silent while contralateral MVN neurons have markedly raised background discharge rates (Smith & Curthoys, 1988a & b). Within a week, as behavioural symptoms subside, similar firing rates between the ipsi- and contralateral sides are re-established. (Ris *et al.*, 1995). It is this correlation between behaviour and neuronal activity that made the vestibular nuclei a proposed site for compensation. Studies have shown that there are significant commissural inhibitory inputs between the two MVN and they may play an important role in compensation by restoring firing rate after unilateral vestibular loss. Therefore, we have investigated whether there are changes in inhibitory GABAergic and glycinergic quantal synaptic transmission during vestibular compensation.

Methods. *Unilateral Labyrinthectomy:* All experiments were conducted according to The University of Newcastle Animal Care and Ethics Committee Regulations. Mice (C57BL6) approximately 4 weeks old underwent UL in a procedure described by Gacek & Khetarpal (1998). Under isoflurane anaesthetic, both the horizontal and anterior ampullae were removed, the vestibule was filled with Gelfoam and the surgical incision closed using interrupted sutures. Animals recovered after anaesthetic and immediately displayed behavioural symptoms consistent with UL. *In vitro slice preparation:* At three time points following UL (4 hours, 2 days and > 7 days), mice were anaesthetised using Ketamine (100 mg/kg, i.p) and decapitated. Brainstem sections were prepared as previously described (Camp *et al.*, 2006). Post-mortem examination of the bony labyrinth confirmed the removal and destruction of the ampullae. *Whole-cell patch-clamp recordings*: Glycine and $GABA_A$ receptor mediated quantal synaptic currents were recorded using CsCl-based internal solution and in the presence of various antagonists including tetrodotoxin (1 μM), CNQX (10 μM), bicuculline (5 μM) and strychnine (1 μM).

Results & Discussion. Inhibitory quantal currents were recorded from a total of 157 MVN neurons. We measured quantal amplitude, rise time, decay time and frequency from neurons in the ipsi-lesioned and contra-lesioned MVN. Our results show that there are no significant changes in GABAergic quantal events (including amplitude, kinetics or frequency) between ipsilesional, contralesional, or control medial vestibular nucleus neurons (MVNn) at any time point investigated after UL. In contrast, we have found a significant increase at 4 hours after UL, in the amplitude and frequency of glycine receptor mediated mIPSCs from contra-lesioned MVNn (amplitude: 70.2 ± 16.1pA, $p < 0.05$; frequency: 0.7 ± 0.2 Hz, $p < 0.05$) and an increase in the frequency of mIPSCs in ipsi-lesioned MVNn (frequency: 0.6 ± 0.2 Hz, $p < 0.05$) compared to control MVNn (amplitude: 37.3 ± 6.6 pA; frequency 0.2 ± 0.03 Hz). Since there were no changes in glycinergic mIPSC kinetics, increases in amplitude were not due to receptor subunit changes. Therefore our results suggest that GABAergic synaptic transmission has a limited role in MVNn during early vestibular compensation. In contrast, fast inhibitory synaptic transmission mediated by glycine receptors plays a significant a role in altering neuronal excitability during early vestibular compensation.

Camp AJ, Callister RJ & Brichta AM. (2006) *Journal of Neurophysiology*, **95:** 3208-18.
Gacek RR & Khetarpal U. (1998) *Laryngoscope* **108:** 671-8.
Ris L, de Waele C, Serafin M, Vidal PP & Godaux E. (1995) *Journal of Neurophysiology*, **74:** 2087-99.
Smith PF & Curthoys IS. (1988a) *Brain Research*, **444:** 295-307.
Smith PF & Curthoys IS. (1988b) *Brain Research*, **444:** 308-19.

Funding provided by NHMRC, Garnett Passe and Rodney Williams Memorial Foundation and HMRI

A horizontal spinal cord slice preparation for studying descending synaptic inputs to neurons in the mouse spinal cord

J.R. Flynn,[1] M.P. Galea,[2] A.M. Brichta,[1] R.J. Callister[1] and B.A. Graham ,[1] [1]School of Biomedical Sciences, University of Newcastle, Callaghan, NSW 2308, Australia and Hunter Medical Research Institute (HMRI), New Lambton, NSW 2305, Australia and [2]School of Physiotherapy and Rehabilitation Sciences Research Centre, The University of Melbourne, Melbourne, VIC 3010, Australia.

Since the introduction and widespread use of *in vitro* spinal cord slice preparations, studies of evoked synaptic transmission in spinal neurons have concentrated on inputs from two sources; those from primary afferents and local circuit neurons. This focus is due largely to practical considerations. For example, peripheral inputs can be readily activated by stimulation of dorsal roots that often remain attached to spinal cord slices. Similarly, local inputs can be studied within a slice by low intensity focal stimulation of visualized neurons or even recording from pairs of neurons. The other major source of synaptic input to the spinal cord, from more distant propriospinal, brainstem, midbrain and even cortical regions, has been overlooked in slice work because of the difficulty of maintaining the integrity of long descending axons in a spinal cord slice. A preparation that enables study of descending synaptic connections is now needed as recent studies suggest that it is possible for regenerating axons to regrow across a spinal cord lesion (Goldshmit *et al.*, 2004). So far these studies have only presented anatomical and behavioural evidence for successful axon regrowth across spinal cord lesions. It is not known if sprouting or regenerating axons make functional synaptic connections with neurons above or below the lesion site. Accordingly, we have taken advantage of the small size of the mouse spinal cord to develop a horizontal spinal cord slice preparation that permits investigation of synaptic transmission at connections between descending axons and spinal neurons. Mice (C57Bl/6; both sexes, aged 19 - 41 days) were anaesthetised with Ketamine (100 mg/kg, i.p.) and decapitated. A length of spinal cord spaning from mid-thoracic (~ T8) to mid-lumbar (~ L4) segments was removed and glued ventral side down onto a cutting stage. The stage was oriented in a cutting chamber to allow cutting of horizontal slices (300 μm thick). A substantial length of cord containing midline fibre tracts (dorsal columns) could be retained in at least two slices. Patch clamp recordings (KCH_3SO_4 internal) were made in neurons in the dorsal grey matter. These recordings were most likely made in the superficial and deep dorsal horn regions in the first and second slice, respectively. Synaptic responses were evoked in dorsal horn neurones by stimulating the dorsal columns with a bipolar electrode (200 μm tip separation) at various distances rostral to the recording site. Responses were evoked in 26 of 32 recordings with success highly dependent on the distance between stimulating and recording site (0 to 500 μm = 75%; 500 to 1000 μm = 94%; 1000 to 1500 μm = 86%; and 1500 to 2000 μm = 33%). In voltage-clamp (holding potential -60 mV), three different types of response that exhibited constant latency and low failure rate after stimulation at 1.2 × threshold were distinguished: single component monosynaptic (15/26); dual component monosynaptic (8/26); and multi component polysynaptic (3/26). Subsequent current clamp recordings in a subset of neurones (13/26) revealed that some evoked responses contained an inhibitory component (5/13). Some neurones (13/25) receiving evoked synaptic inputs were also categorized according to their discharge patterns during depolarising current step injection (800 ms, 20 pA steps): Tonic firing (5/13); initial bursting (6/13); and delayed firing (2/13). In summary, these data indicate that a variety of descending synaptic inputs, which travel in the dorsal columns, can be preserved in horizontal slices of the mouse spinal cord. These descending inputs can be excitatory or inhibitory and innervate a heterogeneous population of target neurones in the superficial and deep dorsal horn. This information shows that horizontal spinal cord slices in the mouse may in future provide a model to assess the functional relevance of anatomical regrowth across spinal cord lesions.

Goldshmit Y, Galea MP, Wise G, Bartlett PF & Turnley AM. (2004) *Journal of Neuroscience,* **24:** 10064-73.

Effects of a cognitive task on sway and postural reflex activity during standing

B.L. Julien and A.P. Bendrups, School of Human Biosciences, La Trobe University, VIC 3086, Australia.

We investigated the effects of a cognitive task, the Stroop Test, on the postural reflex activity and sway of eleven healthy adults using a protocol which controlled for the confounding factors of visual fixation and articulation. The Stroop Test consists of the words red, green and blue printed in incongruent ink (*e.g.* "red" printed in green); the task is to respond with the colour of the ink and not to read the word. Subjects performed the Stroop Test or a control reading task when either standing at ease with a wide base of support (BOS) or standing still with a narrow BOS. A measure of postural reflex activity was provided by stiffness at the ankle using a modified version (see Ho & Bendrups, 2002) of the protocol developed by Fitzpatrick *et al.* (1992). Ankle stiffness values were obtained from recordings of ankle torque and ankle angle in response to unperceived forward pulls and expressed as a ratio of the load stiffness, yielding the 'reflex stiffness' (see the Table). Postural sway was obtained from the SD of the body position data (see the Table). Under both postural conditions, mean sway was significantly lower during Stroop Test performance compared to control (two-way repeated measures analysis of variance, $p = 0.007$). There was no significant effect of the Stroop Test on mean reflex stiffness under either postural condition.

Postural condition	**Measure**	**Control**	**SD**	**Stroop**	**SD**
Ease with wide BOS	Sway (deg)	0.122	0.042	0.100	0.032
	Reflex stiffness	1.38	0.301	1.63	0.480
Still with narrow BOS	Sway (deg)	0.115	0.038	0.104	0.036
	Reflex stiffness	1.61	0.488	1.58	0.420

Subsequently, physiological and psychological variables were recorded in subjects performing the Stroop Test while seated, to seek an explanation for the between-subject variability in reflex stiffness. Increased heart rates during Stroop Test performance suggest that this task increased physiological arousal. The subjective difficulty of the Stroop Test influenced the direction of its effect on stiffness when subjects stood at ease with a wide BOS: subjects who rated the Stroop Test as being difficult had decreased stiffness and those who rated the Stroop Test as easy had increased stiffness. Both respiration rate and resting gastrocnemius activity were correlated with changes in sway during Stroop Test performance. Subjects with higher respiration rates when seated had greater postural sway when standing still with a narrow BOS, consistent with Jeong (1991). Subjects with higher gastrocnemius activity while seated had increased sway when standing at ease with a wide BOS, suggesting that this increased muscle tone may have had a destabilising effect. We hypothesised that there would be an inverse relation between stiffness and sway. However, the results show that performing the Stroop Test improved postural stability (decreased sway) without necessarily increasing stiffness.

Fitzpatrick R, Taylor J & McCloskey D. (1992) *Journal of Physiology*, **454:** 533-47.

Ho CY & Bendrups AP. (2002) *The Journals of Gerontology Series A, Biological Sciences and Medical Sciences*, **57A:** B344-50.

Jeong BY. (1991) *Archives of Physical Medicine and Rehabilitation*, **72:** 642-5.

N-type calcium channels contribute to acetylcholine release from parasympathetic but not sympathetic preganglionic neurons in female mice

P. Jobling, School of Biomedical Sciences and Hunter Medical Research Institute, University of Newcastle, Callaghan, NSW 2308, Australia.

Neurons communicate with each other almost exclusively through chemical synapses *via* a mechanism that is dependent on calcium. The link between calcium entry into the nerve terminal and neurotransmitter release has been the subject of considerable study over recent decades. Whilst many of the underlying principles common to all synapses have been elucidated, it is becoming increasingly apparent that the relationship between calcium entry and synapse function varies considerably between synapses. Of particular note is differential expression of calcium channel subtypes which provide the source of calcium necessary for neurotransmitter release. The reasons for such diversity are unclear. Perhaps they allow the vastly different patterns of communication which we see in different neural circuits? As in the central nervous system, peripheral synapses which control autonomic targets show heterogeneity in the calcium channel subtypes they express. Outflow from any particular autonomic pathway is the culmination of activity from a number of nuclei in the brainstem, hypothalamus and higher areas. In turn these activate preganglionic neurons within the spinal cord. Preganglionic neurons in certain pathways, especially those which control reproductive tissues, also participate in reflex circuits regulated at the level of the spinal cord. Preganglionic outflow is relayed to peripheral effectors through synapses in autonomic ganglia. It is now clear that the autonomic pathways controlling different effectors are independently regulated. The fact that each autonomic pathway and hence ganglionic synapse has characteristic patterns of activation suggests that transmitter release may be optimally "tuned" to the requirements of the end organ. In a previous study we demonstrated that in paracervical ganglia of female guinea-pigs acetylcholine (ACh) release from the terminals of sacral preganglionic neurons requires calcium entry from both N-type calcium channels and an undetermined calcium channel, possibly R-type. In contrast, N-type calcium channels play no role in acetylcholine release from the terminals of lumbar preganglionic neurons in the same ganglion (Jobling *et al.*, 2004). One difference between N-type calcium channels and other calcium channel subtypes is that N-type calcium channels are modulated to a greater extent by G-protein coupled receptors. Perhaps the selective involvement of N-type calcium channels in sacral pathways confers greater synaptic plasticity? To determine if our result represents a general mammalian phenomenon we have now investigated the functional role of calcium channels in transmitter release from parasympathetic and sympathetic terminals in paracervical and prevertebral ganglia of female mice. Pelvic or celiac ganglia were taken from mice (3-5 weeks of age) killed under deep anaesthesia following intraperitoneal injection of sodium pentobarbitone (150 mg/Kg). These procedures were approved by the Animal Welfare Committee of the University of Newcastle in accordance with the National Health and Medical Research Council Australian code of practice for the care and use of animals for scientific purposes. Ganglia were pinned in a recording chamber and superfused with HEPES buffered salt solution. Intracellular recordings were made with microelectrodes filled with 0.5 M KCl. Pelvic nerves to paracervical ganglia or splanchnic nerves to celiac ganglia were stimulated via suction electrodes. Preganglionic nerve stimulation evoked suprathreshold EPSPs in the majority of postganglionic neurons. In order to better resolve pharmacological effects of calcium channel antagonists, hexamethonium (30-100μM) was routinely used to reduce the amplitude of EPSPs below threshold. Single electrode voltage-clamp was used to measure EPSC amplitude in the absence and presence of selective calcium channel antagonists. In paracervical ganglia omega conotoxin GVIA, a selective N-type calcium channel antagonist, reduced the amplitude of EPSCs evoked by pelvic nerve stimulation by ($46 \pm 5\%$, $n = 8$), $p < 0.05$). In contrast, in the celiac ganglion, omega conotoxin GVIA had no effect on the amplitude of EPSCs evoked by splanchnic nerve stimulation ($P = 0.2$, $n = 7$). EPSCs in both paracervical and celiac ganglia were resistant to the P-type calcium channel antagonist agatoxin (50 nM, $n = 5$ paracervical, $n = 5$ celiac) and the R-type calcium channel antagonist SNX482 (100 nM, $n = 4$ paracervical, $n = 4$ celiac). These results indicate that in the female mouse, release of ACh from sacral parasympathetic preganglionic neurons requires calcium entry from both N-type and toxin-resistant calcium channels. Release of ACh in sympathetic pathways to prevertebral ganglia does not require calcium entry from N-type calcium channels. The expression of N-type calcium channels in sacral preganglionic neurons may provide a mechanism for selective modulation of these pathways.

Jobling P, Gibbins IL, Lewis, RJ, & Morris JL. (2004) *Neuroscience*, **127:** 455-86.